A role for autophagy of the ER in rejuvenation revealed by microfluidics-based lifespan profiling of yeast gametes

Silvan Spiri[1]*, Tina Lynn Sing[1], Nhi Phung[1], Jay S Goodman[1], Elçin Ünal[1,2,3]* & Gloria Ann Brar[1,2,3]*

[1]Department of Molecular and Cell Biology, University of California, Berkeley, Berkeley, CA, 94720, USA
[2]California Institute for Quantitative Biosciences (QB3), University of California, Berkeley, CA, 94720, USA
[3]Center for Computational Biology, University of California, Berkeley, Berkeley, CA 94720, USA

*Correspondence: silvan.spiri@berkeley.edu, elcin@berkeley.edu, gabrar@berkeley.edu

Key words: gametogenesis, rejuvenation, lifespan, microfluidics, autophagy, *Saccharomyces cerevisiae*, meiosis, yeast, ERphagy.

Abstract

During mitotic growth, *Saccharomyces cerevisiae* cells age by dividing asymmetrically producing young daughter cells while retaining age-associated damage in the mother cell, which will eventually become senescent. Gametogenesis naturally and completely resets precursor cell lifespan, even for replicatively aged cells but so far, no cellular mechanism responsible for this rejuvenation has been identified. This is in part due to the existing methods to quantify replicative lifespan resetting in this context, which are limited to low-throughput and labor-intensive approaches. Here, we introduce a high-throughput microfluidic-based assay that allows systematic characterization of factors required for gametogenic rejuvenation in *S. cerevisiae.* With this technique, we show that we can capture a wide range of gamete replicative lifespans that are consistent with known longevity mutants. Excitingly, using this technique, we report receptors involved in selective autophagy of the ER as the first identified molecular determinants of gametogenic rejuvenation. We anticipate this novel technique will enable systematic identification of additional molecular factors that drive gametogenic rejuvenation.

Introduction

Life is continuously maintained by organisms through the genesis of offspring. In sexually reproducing eukaryotes, gametogenesis is a conserved developmental program that forms haploid gametes from diploid precursor cells. Although somatic cells deteriorate over time, mechanisms exists that eliminate age-associated damage in the germline and during gametogenesis to secure the fitness and survival of the next generation (Gladyshev, 2021; Jones, 2007; Maklakov and Immler, 2016; Smelick and Ahmed, 2005; Yamashita, 2023). Despite the importance of these pathways, the specific molecular mechanisms mediating this programmed developmental rejuvenation remain elusive.

During mitotic growth, *Saccharomyces cerevisiae* divides asymmetrically producing young daughter cells by retaining age-associated damage in the aging mother cell (Denoth Lippuner et al., 2014; Higuchi-Sanabria et al., 2014; Hughes and Gottschling, 2012; Nyström and Liu, 2014). This limits the number of daughter cells that a mother cell can produce (termed "replicative lifespan") before reaching senescence. Excitingly, upon completion of gametogenesis, replicative lifespan of all gametes is completely reset in *S. cerevisiae*, relative to that of the precursor cell (Neiman, 2011; Tina L. Sing et al., 2022; Ünal et al., 2011; Ünal and Amon, 2011) (**Fig. 1**). The portability of this rejuvenation program was demonstrated by the observation that ectopic expression of Ndt80, a transcription factor necessary for completion of gametogenesis, extends replicative lifespan in mitotic cells (Ünal et al., 2011; Xu et al., 1995). Since this initial discovery, there has been interest in factors that are expressed during gametogenesis and that may drive lifespan resetting in gametes (Tina L. Sing et al., 2022). Drug-mediated inhibition of bulk autophagy prevents clearance of age-associated Hsp104 foci during gametogenesis and completion of gametogenesis, suggesting that autophagy mediated turnover of aged proteins and cellular components might play an important role in orchestrating gametogenic rejuvenation (Tyler and Johnson, 2018; Ünal et al., 2011).

Yeast gametogenesis, a highly experimentally tractable process that can be induced efficiently at will, presents the unique opportunity to gain mechanistic insights into the process of germline rejuvenation, but current techniques to quantify replicative lifespan of gametes limit progress in the field. Quantification of replicative lifespan in gametes has relied on scoring cell divisions using manual micromanipulation, with the replicative lifespan of a gamete mother cell being scored over several days by continuous counting and removing of daughter cells using a microdissection microscope (Ünal et al., 2011). This technique is tedious, low throughput and labor intense. In fact, since gametogenesis-specific rejuvenation was initially observed (Ünal et al., 2011), only two other studies have used this technique to measure replicative lifespan of gametes (Koch et al., 2020; Lee et al., 2019) and no specific pathways that directly mediate gametogenic rejuvenation have been found. Although micromanipulation has historically been used to quantify replicative lifespan in vegetatively growing haploid yeast cells (Mortimer and Johnston, 1959), microfluidics-based approaches that increase throughput and lower manual labor have successfully been developed and adopted for yeast lifespan measurement in recent years. Multiple different trap designs have been used to capture and retain mother cells in imaging chambers with a constant media flow over prolonged periods of time. Parallelization of multiple imaging chambers allows acquisition of hundreds of cells from multiple different genetic backgrounds over a few days in one single experiment (Chen et al., 2017; Jin et al., 2019; Jo et al., 2015; Li et al., 2020; Liu et al., 2015; Thayer et al., 2022). Even

though microfluidics-based quantification of replicative lifespan is rapidly replacing micromanipulation-based readouts for vegetatively growing haploid yeast cells, a technique to apply microfluidics-based platforms to investigate the replicative lifespan of gametes does not currently exist. The challenges associated with capturing and measuring gamete lifespan include (i) the need to purify gametes from precursor cells and from the ascus that encloses four gametes together, (ii) the need to prevent mating of neighboring gametes, and (iii) the small size of gametes relative to precursor cells.

To overcome these limitations, here we developed a microfluidic-based microscopy assay that allows high-throughput characterization of factors required for gametogenic rejuvenation in *S. cerevisiae*. We engineered inert genetic modifications and mitigated the aforementioned challenges to enable microfluidic-based assessment of replicative lifespan in *S. cerevisiae* gametes derived from the SK1 background, which undergoes gametogenesis with high efficiency (Kane and Roth, 1974; Padmore et al., 1991). With this approach we were able to isolate and purify single gametes from both young and aged precursor cells, which we imaged over 72 hours using a custom microfluidic device, allowing quantitative analysis of gamete replicative lifespan.

Comparing the replicative lifespan of gametes derived from young versus aged precursor cells using this platform captured a broad spectrum of lifespan outcomes and confirmed effects of known longevity mutants. Most excitingly, using this system, we discovered that turnover of the endoplasmic reticulum (ER) mediated by selective autophagy (ERphagy) but not mitophagy is required during gametogenesis for complete lifespan resetting in aged gametes. ERphagy receptors Atg39 and Atg40 represent the first proteins known to drive natural rejuvenation through gametogenesis, providing a molecular foothold to dissect the impact of ER quality and inheritance in cellular deterioration. Moreover, this discovery points to the promise of our microfluidic approach to uncover new mechanisms by which eukaryotic cells counteract age-associated damage.

Results

Development of an approach for long-term marking of gametes to enable lifespan analysis

PMA2 encodes a plasma membrane proton pump (Carmelo et al., 1997; Saliba et al., 2018; Serrano et al., 1986). Its paralogous protein, Pma1, is highly expressed during vegetative growth, with an exceptionally long half-life and displaying asymmetric retention in mother cells (Henderson et al., 2014). *PMA1* is essential for viability but *PMA2* is not, and is barely detectable during mitotic growth (Fernandes and Sá-Correia, 2003; Schlesser et al., 1988; Serrano et al., 1986). *PMA2* translation and protein levels are upregulated during late gametogenesis (**Fig. S1A-C** (Cheng et al., 2019)). To further investigate the expression pattern of *PMA2*, we created a transgenic reporter strain carrying a Pma2-GFP fusion protein under its endogenous promoter and tracked its expression timing relative to meiotic divisions by using a fluorescently labeled chromatin marker (Htb1-mCherry). Pma2-GFP expression was upregulated 1-2 hours following anaphase II and predominantly localized to the gamete plasma membranes (**Fig. 2A**). Importantly, Pma2-GFP was not detected in cells that fail to undergo gametogenesis (arrows, **Fig. 2A**). Next, we analyzed Pma2-GFP expression in gametes undergoing germination, their first mitotic division. We found that daughter cells from gametes completely lacked Pma2-GFP signal, which was fully retained on the plasma membrane of

gametes for several rounds of cell division (**Fig. 2B**). Our expression pattern analysis revealed that Pma2-GFP is a reliable and specific marker of gametes exhibiting gamete-specific retention beyond germination, making it an optimal reporter to distinguish gametes from vegetative cells or cells that fail to complete gametogenesis.

Cell populations efficiently sorted by age progress robustly through gametogenesis

To assess the ability of our approach to reliably quantify gametogenic rejuvenation, we first separated pre-meiotic diploid cell populations by replicative age using an established protocol (Smeal et al., 1996). Briefly, a founder cell population was biotin labelled with sulfo-NHS-LC-biotin, which specifically and permanently binds to cell surface proteins that are retained in the founder (mother) cells during subsequent mitotic divisions. These biotin-labeled founder cells were then replicatively aged and incubated with anti-biotin magnetic beads that enabled their isolation from the young daughter cells. The labeled cell suspension was sequentially passed through two magnetic columns to increase purity, followed by elution. The first flow-through cells represent the young cell population. The eluate from the second represent the aged cell population (**Fig. 2C &** methods). Sorted cell populations were stained with fluorescent markers visualizing biotin as well as the chitin-rich, ring-like structures called bud scars on the yeast cell wall, one of which is left after each budding event thus revealing the replicative age of a cell (Cabib and Bowers, 1971). We measured the purity as well as the age of the sorted population by fluorescent microscopy to analyze biotin labelling and bud scar number (**Fig. 2D**, left panel). With our consecutive-sort protocol, we consistently obtained pure young (3.63% biotinylated cells with a mean replicative age of 1.16), and aged (96.74% biotinylated cells with a mean replicative age of 8.55) cell populations (**Fig. 2E&F**). We transferred the separated cell populations to media that induces gametogenesis and analyzed efficiency of gametogenesis after 24 hours. We found that 79.8% of young cells and 78.89% of aged cells successfully formed visibly distinct tetrads (**Fig. 2G**) and that gametes from young as well as aged cell population both robustly expressed Pma2-GFP after completion of gametogenesis (**Fig. 2D**, right panel). Furthermore, we re-evaluated the purity as well as the age of the sorted population following gametogenesis and confirmed that relative distributions of young and aged populations was maintained (**Fig. 2H&I**). In summary, we are able to isolate pure young and aged cell populations and find no detectable negative effect of our experimental regime on the efficiency of gametogenesis.

Isolation of single gametes for microfluidics-based replicative lifespan profiling

To be able to assess replicative lifespan of yeast gametes using microfluidic devices we had to overcome three major obstacles. First, we had to circumvent initiation of mating of gametes with different mating types in response to mating pheromones, which leads to growth arrest and abnormal cell morphology. Second the four gametes within a tetrad do not separate during germination (**Fig. 2B**) rendering assessment of replicative lifespan impossible, thus we had to find a way to separate tetrads into single gametes before loading into the microfluidics imaging chambers. Third, separated gametes, which are significantly smaller than vegetative growing cells, do not fit into our custom-built U-traps for vegetatively growing haploid SK1 cells that are found in our microfluidics devices (**Fig S2A-D** adapted from (Jo et al., 2015)).

Cells from the SK1 background are known to form both covalent (mother-daughter cell adherence) and non-covalent (flocculation) interactions, which present an issue when using microfluidics-based application due to elevated clogging. To mitigate this, we introduce a point mutation into *AMN1* to promote efficient mother-daughter cell separation (Fang et al., 2018). We also deleted *FLO8*, a transcription factor required for flocculation (Kobayashi et al., 1996). During gametogenesis, a diploid yeast cell undergoes two meiotic divisions forming a tightly packed tetrad containing four haploid gametes with a 2:2 segregation of the two mating types *MAT*a and *MAT*α (**Fig. 1&3A**). To avoid triggering the mating response in gametes, we replaced the endogenous promoter of the mating response signaling scaffold gene *STE5* (Chol et al., 1994), with an anhydrotetracycline-inducible promoter (**Fig. S2E**) (Bellí et al., 1998). We confirmed sterility and inducible fertility by mixing *MAT*a and *MAT*α cells on control and anhydrotetracycline-containing plates and monitoring the mating response by scoring diploid formation (**Fig. S2F**).

To obtain single gametes and to eliminate cells that did not proceed through gametogenesis, we incubated post-gametogenesis cultures with zymolase. This enzyme hydrolyses the main structural polysaccharide in the cell wall, thus lysing non-gametes and weakening the ascus protecting the gametes (**Fig. 3A**). We then gently sonicated the zymolase-treated tetrads to disassociate them into single gametes and confirmed detectability of the Pma2-GFP marker on single gametes by fluorescence microscopy (**Fig. 3A&B**).

When loading separated gametes directly into our custom microfluidics devices (**Fig S2A-D** adapted from (Jo et al., 2015)), gametes were not retained in the traps due to their small size. To circumvent this issue, gametes were first grown in rich media for 3 hours following their separation, which was long enough for them to increase in size but short enough to only allow the first cell division to occur (**Fig. S2G**). These gametes were then loaded into the microfluidic devices and an image of the whole region of interest was taken in the FITC and brightfield channel. By assessing Pma2-GFP expression, we could reliably determine if a trapped cell was a gamete, or a progeny cell generated during re-growth (**Fig. 3C**). Next to quantify replicative lifespan of gametes, brightfield images were acquired every 15 minutes over 72 hours, capturing every cell division (**Fig. 3D&S2H**). Together, these steps constitute a pipeline that allows for the quantification of gamete replicative lifespan potential, and identification of mutants that specifically impact rejuvenation of aged cells, using a high-throughput microfluidics-based imaging platform (**Fig. 3E**).

Wild-type gametes from aged precursor cells display complete resetting of replicative lifespan

It has previously been shown that replicative lifespan is completely reset after gametogenesis. This study used a micromanipulator continuously counting and removing daughter cells of gametes previously placed onto agar plates and was assessed only in the W303 and A364a strain background (Ünal et al., 2011). Thus, we wanted to test if in our strain background and using our pipeline, gametes also showed a complete reset of their replicative lifespan. Towards this end, we sorted diploid wild-type cells following our established protocol (**Fig. 2C**) and analyzed the replicative age of young and aged pre-gametogenic cell populations (**Fig. S3A&B**). Separated cell populations were transferred to media inducing gametogenesis and after 24 hours both successfully completed gametogenesis (**Fig. S3C**). We analyzed purity of

sorting and replicative age of post-gametogenic tetrads (**Fig. 4A&S3D**), acquired and quantified the replicative lifespan of gametes following our pipeline and found the median replicative lifespan for gametes from young precursor cells was similar to gametes from aged precursors (**Fig. 4B**, p=0.982, Log-rank (Mantel-cox)). An independent biological replica led to a similar outcome (**Fig. S3E-J**). These results confirm that our newly developed high-throughput microfluidic based pipeline can capture and quantify gametogenic rejuvenation.

Microfluidics-based analyses of gamete lifespans capture a wide range of outcomes among known longevity mutants

To test the sensitivity of our system in detecting differences in replicative lifespan potential of gametes, we quantified lifespans of young gametes derived from known longevity mutant backgrounds. Deletion of the gene encoding Sir2, a NAD^+- dependent histone deacetylase, is known to decrease replicative lifespan of yeast by approximately 50% due in part to loss of silencing of the rDNA locus, leading to the generation and accumulation of extrachromosomal rDNA circles (Kaeberlein et al., 1999; Sinclair and Guarente, 1997). On the other hand, deletion of the gene encoding Fob1, an rDNA spacer replication fork barrier binding protein, is reported to extend lifespan in yeast by up to approximately 40%, due to decreased rDNA recombination and thus fewer extrachromosomal rDNA circles (Defossez et al., 1999).

We sorted *sir2*Δ, wild-type, and *fob1*Δ diploid cells (**Fig. 2C**) and analyzed the sorting efficiency and replicative age of the young pre-gametogenic cell populations (**Fig. S3K&L**). We transferred the separated cell populations to media that induces gametogenesis and found after 24 hours 87.3% of *sir2*Δ cells, 90.4% of wildtype cells and 73.7% of *fob1*Δ cells successfully completed gametogenesis (**Fig. S3M**). Upon analyzing purity of sorting and replicative age in tetrads (**Fig. 4C&S3N**), we separated the tetrads into single gametes and acquired their replicative lifespan over 72 hours. We found the median replicative lifespan for gametes derived from young precursor *sir2*Δ cells to be 11, significantly lower than gametes derived from young wild-type cells, with a median lifespan of 21 (**Fig. 4D**, p<0.0001, Log-rank (Mantel-cox)). Gametes derived from young *fob1*Δ precursor cells, on the other hand, had a significantly increased median lifespan of 28 compared to wildtype (**Fig. 4D**, p<0.0001, Log-rank (Mantel-cox)). Thus, the microfluidic platform and workflow that we developed can capture a range of gamete lifespans from young precursor cells with mutations in established longevity-linked genes.

Gametes lacking *SIR2* fail to reset replicative lifespan through a mechanism that is independent of gametogenesis

While testing our pipeline we serendipitously observed that gametes derived from aged *sir2*Δ precursor cells did not display complete resetting of replicative lifespan. We sorted *sir2*Δ pre-gametogenic diploid cells into a young cell population (same data as **Fig. S3K&L**) and an aged cell population (**Fig. S4A&B**). 87.3% (same data as **Fig. S3M**) of the young population and 68.0% of old population completed gametogenesis after 24 hours (**Fig. S4C**). We verified purity and replicative age of post-gametogenic cell populations before measuring their lifespan (**Fig. 4E&S4D,** same data as shown in **Fig. S3N&4C** for young). Strikingly, the replicative lifespan of gametes derived from aged *sir2*Δ precursor cells revealed a median replicative lifespan of 8, significantly lower than for gametes derived from young *sir2*Δ precursor cells,

which had a median lifespan of 11 (same data as shown in **Fig. 4D**) (**Fig. 4F**, p<0.0001, Log-rank (Mantel-cox)).

To test whether ectopic expression of *SIR2* during gametogenesis can rescue the lack of replicative lifespan resetting observed in *sir2*Δ cells, we constructed *sir2*Δ strains containing a *SIR2* ORF transgene under the control of a *RIM4* promoter fragment, which is activated during gametogenesis (**Fig. S4E**) and confirmed gametogenesis-specific expression (**Fig. S4F**) (Cheng et al., 2018; Deng and Saunders, 2001). We then sorted pre-gametogenic diploid *sir2*Δ cells carrying this rescue construct into a young and an aged cell population and determined completion of gametogenesis after 24h (**Fig. S4G-I**). We verified purity and replicative age of sorted cell populations upon gametogenesis before analyzing replicative lifespan of gametes (**Fig. 4G&S4J**). Gametes derived from aged *pRIM4-SIR2 sir2*Δ precursor cells showed a median replicative lifespan of 10, which was still significantly lower than gametes derived from young *pRIM4-SIR2 sir2*Δ cells, with a median lifespan of 17 (**Fig. 4H**, p<0.0001, Log-rank (Mantel-cox)). We note a slightly increased replicative lifespan of gametes derived from both young and old *pRIM4-SIR2 sir2* precursor cells compared to those derived from *sir2*Δ cells, which may be due to residual Sir2 protein observed in late gametes that could carry over through the first cell divisions (**Fig. S4F**, right most band). In summary, we show that *sir2*Δ gametes do not completely reset their lifespan following gametogenesis, however, this phenotype cannot be rescued by providing Sir2 during gametogenesis. This suggests that aged *sir2*Δ cells might accumulate damage that cannot be cleared by the gametogenic rejuvenation program.

Selective Autophagy is necessary to reset replicative lifespan during gametogenesis

Autophagy mediates lysosomal degradation of damaged organelles and proteins (Mizushima et al., 2008). Autophagy pathways decline during aging, leading to loss of proteostasis and accumulation of cellular damage. Artificially increasing autophagy factors can lead to lifespan extension (Hansen et al., 2018; Rubinsztein et al., 2011; Simonsen et al., 2008; Tyler and Johnson, 2018). Both Atg1, an essential kinase required for initiation of autophagosome formation, and Atg8, which is required for formation of the autophagosome membrane, are upregulated during gametogenesis (**Fig. 5A&B; S5A-D**) (Cheng et al., 2018; Ichimura et al., 2000; Matsuura et al., 1997). In yeast, the general autophagy machinery is essential for meiotic entry as well as progression, which hinders evaluating the effect of bulk autophagy on gamete rejuvenation (Neiman, 2005; Tsukada and Ohsumi, 1993; Wen et al., 2016). Atg11, the main selective autophagy scaffold protein required for Atg1 recruitment to specific selective autophagy receptors is also dynamically upregulated during gametogenesis (**Fig. 5C; S5E&F**) and we found that cells deleted for Atg11 can undergo gametogenesis (Cheng et al., 2018; Farré and Subramani, 2016; Kamber et al., 2015). Thus, we tested if cellular quality control via selective autophagy plays a direct role in gametogenic rejuvenation by deleting *ATG11* and measuring their rejuvenation potential with our established pipeline.

We sorted pre-gametogenic cells into young and aged cell populations and 24h after induction verified efficiency of gametogenesis (**Fig. S5G-I**). Replicative age of tetrad population was verified by quantifying bud cars per tetrad and number of biotinylated tetrads in the population (**Fig. 5D&S5J**, Rep.1). Excitingly, when quantifying the replicative lifespan of gametes, we found a significant difference between cells from aged and young *atg11*Δ precursor cells that

was highly reproducible (**Fig. 5E**, Rep.1, p<0.0001, Rep.2, p<0.0001, Log-rank (Mantel-cox), compare to **Fig. 4B**). This result suggests that Atg11-mediated selective autophagy is essential for full rejuvenation of gametes derived from aged precursor cells.

Mitophagy is not necessary to reset replicative lifespan during gametogenesis

Atg11 recruits the autophagy machinery upon binding to specific selective autophagy receptors that mark different organelles for degradation, thus we wondered if selective autophagy of a specific compartment is necessary for gametogenic rejuvenation. To address this, we first investigated a potential role for Atg32, an autophagy receptor localized on the outer mitochondria membrane that mediates selective removal of damaged and excess mitochondria via mitophagy (Kanki et al., 2009; Kondo-Okamoto et al., 2012; Okamoto et al., 2009). Atg32 is strongly upregulated in mid-meiosis (**Fig. S6 A-C** (Cheng et al., 2018)) and specific mitochondrial remodeling and inheritance during gametogenesis has been described before (Sawyer et al., 2018; Suda et al., 2007).

We deleted *ATG32* in diploid cells and tested their gametogenic rejuvenation potential. We again sorted pre-gametogenic cells into young and aged cell populations, determined efficiency of gametogenesis and analyzed biotin label and replicative age of post gametogenic cell populations (**Fig. S6D-H**). No significant difference of replicative lifespan was observed between gametes from aged compared to young *atg32*Δ precursor populations (**Fig. S6I**, p=0.2691, Log-rank (Mantel-cox)). *ATG33,* localized on the outer mitochondria membrane also confers selectivity during mitophagy under certain growth conditions and is upregulated during meiosis (**Fig. S6J-L**). To exclude that *ATG33* mediated mitophagy acts in parallel thereby masking a possible rejuvenation phenotype of *atg32*Δ mutants we created *atg32*Δ *atg33*Δ double mutants and tested their rejuvenation potential. We age-sorted *atg32*Δ *atg33*Δ double mutant pre-gametogenic cells into young and aged cell populations, determined efficiency of gametogenesis and analyzed biotin label and replicative age of post gametogenic cell populations (**Fig 5F & S6M-P**). Like in *atg32*Δ cells, no significant difference in replicative lifespan was observed in *atg32*Δ *atg33*Δ double mutant gametes (**Fig. 5G**, p=0.7414, Log-rank (Mantel-cox)). These experiments suggest that selective mitophagy is dispensable for gametogenic rejuvenation. Intriguingly, failure of *atg32*Δ *atg33*Δ to phenocopy *atg11*Δ implies that only a specific arm of selective autophagy mediated by Atg11 is necessary for gametogenic rejuvenation.

ERphagy is necessary for full gametogenic lifespan resetting

It has previously been shown that selective autophagy mediated by the autophagy receptors Atg40, and to a lesser extent Atg39, control ER inheritance during gametogenesis. Atg40, and Atg39 are upregulated during gametogenesis (**FigS7 A-F**) and meiotic remodeling of the ER combined with ERphagy prevent specific subpopulations of the ER from being passed onto gametes. It has been proposed that these pathways constitute a quality control mechanism to ensure gametogenic rejuvenation, however this has not been directly tested (Otto et al., 2021; Otto and Brar, 2022).

To determine if Atg39, a transmembrane autophagy receptor in the perinuclear ER mediating nucleophagy impacts gametogenic rejuvenation, we first sorted diploid *atg39*Δ cells into a young and aged cell population (**Fig. S7G&H**) (Mochida et al., 2015). In the young and

aged populations, 70.0% and 82.0% completed gametogenesis, respectively (**Fig S7I**). We verified age separation of post-gametogenic populations before measuring lifespan of gametes with our microfluidic devices (**Fig. S7J&K**). We found no significant difference for replicative lifespan of *atg39*Δ gametes derived from aged precursors with a and *atg39*Δ gametes derived from young precursors (**Fig. S7L**, p=0.418, Log-rank (Mantel-cox)).

Next, we checked if gametogenic reset of replicative lifespan is impaired in cells lacking Atg40, an autophagy receptor localized at the cortical and cytoplasmic ER mediating fragmentation and encapsulation of ER subdomains (Mochida et al., 2015). *atg40*Δ pre-gametogenic mutant cells were sorted into young and aged cell populations, efficiency of gametogenesis as well as biotin label and replicative age of post gametogenic cell populations was determined upon gametogenesis (**Fig S7M-Q).** Similar to *atg39*Δ cells, no significant difference in replicative lifespan was observed between *atg40*Δ gametes derived from aged precursors and *atg40*Δ gametes derived from young precursors (**Fig. S7R**, p=0.389, Log-rank (Mantel-cox)).

Because there is known functional redundancy between Atg39 and Atg40 (Mochida et al., 2015; Otto et al., 2021), we tested if *atg39*Δ *atg40*Δ cells were still capable of completely resetting replicative lifespan during gametogenesis. We determined purity and replicative age upon sorting *atg39*Δ *atg40*Δ diploid cells into young and aged populations (**Fig. S8A&B**, Rep.1). Upon gametogenesis, we determined efficiency of gametogenesis and reassessed sorting purity as well as replicative age (**Fig 5H** and **S8C&D**, Rep.1). Excitingly, lifespan analysis of aged gametes from aged *atg39*Δ *atg40*Δ precursor cells revealed a significantly reduced median replicative lifespan compared to gametes from young precursor cells (**Fig 5I**, Rep.1, p=0.0030, Log-rank (Mantel-cox)). This failure to fully rejuvenate aged *atg39*Δ *atg40*Δ gametes was highly reproducible (**Fig. 5H&I**, Rep.2, p=0.0080, Log-rank (Mantel-cox); **S8A-D**). Together, these data revealed that Atg39 and Atg40 both contribute through partially redundant mechanisms to gametogenic rejuvenation, and that full replicative lifespan resetting during gametogenesis depends on the presence of these selective ERphagy receptors.

Meiosis specific expression of *ATG40* is sufficient to rescue resetting of replicative lifespan in aged ERphagy-deficient cells

To determine whether this difference in replicative lifespan between gametes from aged and young *atg39*Δ *atg40*Δ precursor cells is due to lack of selective ERphagy specifically during gametogenesis, we tested if ectopic meiotic expression of *ATG40* is sufficient to rescue it. We constructed *atg39*Δ *atg40*Δ double mutant with the *ATG40* ORF under the control of a *NDT80* promoter fragment, which displays meiosis-specific expression (**Fig. S9A**) as well as a *atg39*Δ *atg40*Δ double mutant control strain (Xu et al., 1995). We confirmed gametogenesis-specific expression by immunoblotting (**Fig. S9B**) and performed rejuvenation assays in independent duplicates.

First, we sorted pre-gametogenic *atg39*Δ *atg40*Δ control cells into young and aged cell population and determined efficiency of gametogenesis (**Fig. S9C-E**). We then analyzed percentage of biotin labeled tetrads and replicative age of post gametogenic cell populations (**Fig 6A, S9F**). Lifespan analysis confirmed again a similar significant and reproducible lower median replicative lifespan in gametes from aged precursor *atg39*Δ *atg40*Δ control cells compared to gametes from young precursor cells (**Fig. 6B**, Rep. 1, p<0.0001, Rep. 2, p<0.0001,

Log-rank (Mantel-cox)). Next, we sorted pre-gametogenic *atg39*Δ *atg40*Δ *pNDT80-ATG40* cells into young and aged cell population, determined efficiency of gametogenesis and confirmed construct expression (**Fig. 6C, S8G-J**). After completion of gametogenesis, we confirmed percentage biotinylated tetrads and mean replicative age of young and aged populations (**Fig 6D&S9K**). Excitingly, there was reproducibly no significant difference of replicative lifespan in gametes from aged precursor *atg39*Δ *atg40*Δ *pNDT80-ATG40* cells, (**Fig. 6E**, Rep.1, p=0.4519, Rep.2, p=0.9538, Log-rank (Mantel-cox)). Together, these experiments demonstrate that complete resetting of replicative lifespan by gametogenesis is dependent on selective ERphagy during this process (**Fig. 6F**).

Discussion

Here we present a new method to identify the molecular mechanisms underlying the natural cellular rejuvenation that accompanies gametogenesis in budding yeast cells, using a high throughput microfluidics platform. This technique accelerates investigations of gametogenic rejuvenation efficiency and will be crucial to reveal further mechanistic insights into the conserved process of gametogenic rejuvenation. Using our microfluidics-based platform, we demonstrate that replicative lifespan completely resets after gametogenesis, corroborating previous reports using microdissection assays as a readout (Ünal et al., 2011). Analysis of gamete lifespan in known longevity mutants reveals a large dynamic range of measurement using this approach. We found that in *sir2*Δ gametes from aged precursor cells, replicative lifespan was not fully reset due to a gametogenesis-independent mechanism. Finally, using this method we revealed that in contrast to Atg32 and Atg33, autophagy receptors involved in mitophagy, the combined function of Atg39 and Atg40, two ER-associated selective autophagy receptors, is necessary for gametogenic rejuvenation. The reconstitution of Atg40 during meiosis in this background is sufficient to completely reset replicative lifespan of aged gametes.

The custom microfluidic devices presented here, with an open U-trap design, can capture a wide dynamic range of replicative lifespan with lower confinement of cells in space compared to other trap designs that can lead to negative effects on longevity due to compression of cells (Gao et al., 2020). This open design presents the drawback that cells might undergo ejection prematurely before senescence can be observed, due to either a significant increase of cell size during the last few divisions of replicative life or due to minor pressure aberrations in the fluidics system over time. To avoid biases when evaluating replicative lifespan of gametes, we counted every gamete that was loaded at the start of our time lapse and classified cells that ejected as censored subjects during analysis (see methods). Following this approach, we can consistently and robustly measure replicative lifespan. We find the quantified increase of 33.33% in median lifespan of young *fob1*Δ gametes and 52% decrease for *sir2*Δ compared to lifespan of young wild-type gametes to be within the range of previous reports (Kaeberlein et al., 2004; Defossez et al., 1999; Kaeberlein et al., 1999).

SIR2 is a well characterized conserved histone deacetylase of the Sirtuin family and regulates replicative lifespan by silencing the ribosomal DNA locus (Kaeberlein et al., 1999; Sinclair and Guarente, 1997). Deletion of the *SIR2* leads to increased rDNA recombination and broad chromosome instabilities due to destabilization of the rDNA locus (Ide et al., 2010; Kobayashi et al., 2004; Kobayashi and Ganley, 2005). We found that gametes from aged *sir2*Δ

precursor cells failed to reset replicative lifespan, a phenotype that could not be rescued by gametogenesis-specific expression of Sir2. One plausible explanation for this is that due to elevated recombination, aged *sir2*Δ cells accumulate chromosomal aberrations, which cannot be corrected during gametogenesis, and are propagated to gametes, thus reducing their life expectancy. Elevated pre-existing damage in *sir2*Δ cells is consistent with the substantially reduced efficiency of gametogenesis in aged cells in this background (**Fig. S4C**) (Boselli et al., 2009), which was not generally observed in other backgrounds we analyzed.

Autophagy of specific cellular components is known to be an important mechanism for cells to counteract age associated damage and delay senescence (Hansen et al., 2018; Rubinsztein et al., 2011; Simonsen et al., 2008; Tyler and Johnson, 2018). The general autophagy machinery is upregulated during gametogenesis and necessary for meiotic entry and progression (Neiman, 2005; Wen et al., 2016). We found that selective autophagy is a crucial pathway to mediate gametogenic rejuvenation and show specificity of this process as ERphagy but not mitophagy is particularly important for gamete rejuvenation.

Specific mitochondrial remodeling and inheritance during gametogenesis has been described (Sawyer et al., 2018; Suda et al., 2007). However, gametes from aged *atg32*Δ *atg33*Δ precursor cells completely reset replicative lifespan, confirming that Atg32 and Atg33-mediated selective autophagy is not necessary for gametogenic rejuvenation. These findings suggest that dedicated mitochondrial quality control may be dispensable for gametogenic rejuvenation. Alternately, autophagy-independent mechanisms such as sequestration of damaged mitochondria via the gametogenic uninherited compartment may ensure inheritance of healthy mitochondria (King et al., 2019). Both scenarios will be interesting to address in future studies using our method.

Developmentally programmed ER remodeling followed by selective autophagy of ER components regulates ER inheritance during yeast gametogenesis (Otto et al., 2021; Otto and Brar, 2022). ER-specific autophagy receptors Atg40 and Atg39, localized on the cortical ER and perinuclear ER, respectively, control this process (Mochida et al., 2015). *atg40*Δ but not *atg39*Δ cells fail to degrade cortical ER components via autophagy during gametogenesis and *atg39*Δ cells show reduced autophagy-mediated loss of cortical and perinuclear ER proteins. Intriguingly, *atg40*Δ *atg39*Δ double mutants have an additive effect on ER protein degradation (Otto et al., 2021). We show that aged *atg40*Δ *atg39*Δ precursor cells fail to produce gametes with a fully reset lifespan. Loss of Rer1, a membrane protein retrieving receptor that maintains ER compartmentalization, has been shown to extend replicative lifespan in vegetative yeast through elevated autophagy triggered by ER stress (Ghavidel et al., 2015; Sato et al., 1997). Thus, we speculate that the observed rejuvenating defect of ERphagy-deficient cells could be caused by the failure to meiotically clear damaged and aggregated ER components that accumulated in aged cells, an interesting area to investigate in future studies.

ERphagy is functionally conserved from yeast to metazoans and essential to maintain ER quality (Dikic and Elazar, 2018). In mammals, mutations in ERphagy receptor FAM134B cause hereditary sensory neuropathy and impaired ER turnover has been linked to neurodegeneration, including Parkinson`s disease (Kim et al., 2023; Murphy et al., 2012). Thus, ER quality control mediated by autophagy is a conserved mechanism to preserve cellular fitness, and our finding suggests that, by assuring ER integrity, meiotic ERphagy contributes to gamete rejuvenation.

As demonstrated, the technique presented here significantly increases feasibility and throughput to identify molecular factors that mediate cellular rejuvenation during gametogenesis in budding yeast cells, thereby enabling new insights into this conserved process that may be broadly informative. To gain a more mechanistic and temporal understanding, this assay can easily be combined with auxin inducible degradation of factors of interest and simultaneous imaging of established aging biomarkers in gametes that fail to completely rejuvenate. An important future goal will be to determine if newly identified rejuvenation factors that control gamete quality are sufficient to extend replicative lifespan in mitotic cells, and to test if they have a conserved function in combating aging in other systems.

Materials and Methods

Yeast strains and plasmids:

Standard molecular methods were used to transform and generate all yeast strains, which were derived from the SK1 background. Specific genotypes, plasmids and primers used to generate strains are listed in Supplementary information (**Tables 1-3**). Deletions were generated by homology directed replacement of ORFs with selection cassettes (Longtine et al., 1998; Powers et al., 2022). The *pPMA2-Pma2-GFP* transgene plasmid was generated by Gibson assembly of the *PMA2* promoter and ORF region, amplified from genomic DNA, with an in frame *GFP*-containing *TRP1* single integration vector (Gibson et al., 2009). The *pTet07.1-STE5* promoter swap was generated by amplifying a *NatR-Tet07.1* fragment using primers that introduced homology for the *STE5* locus (Bellí et al., 1998; Longtine et al., 1998). The *pRIM4-SIR2-V5* rescue construct was generated by Gibson assembly of the *SIR2* ORF region with *pRIM4* and *V5* containing *LEU2* single integration vector (Gibson et al., 2009). The *pNDT80-ATG40-V5* rescue construct was generated by Gibson assembly of the *ATG40* ORF region with *pNDT80* and *V5* containing *LEU2* single integration vector (Gibson et al., 2009). Generated plasmids were assembled using Hifi DNA assembly mix (NEbuilder Hifi DNA Assembly Master Mix, E2621L). *PRNR2-TetR-TUP1, PtetO7.1-TetR* adapted from (Azizoglu et al., 2021) was cloned into a *URA3* single integration vector by Gibson assembly (Gibson et al., 2009). Single integration plasmids were linearized with PmeI (New England Biolabs) mediated restriction digest before transformations and integrations were verified by PCR and sanger sequencing. Generated strains and plasmids are available upon request. The following alleles were constructed in previous studies: *atg39*Δ*, atg40*Δ*, ATG40-3V5* (Otto et al., 2021)*, HTB1-mCherry (Matos et al., 2008), flo8, amn1*^{D368V}*(Tina L Sing et al., 2022)*.

Media and growth conditions

Unless otherwise indicated, diploid cells were grown in YPD (1% yeast extract, 2% peptone, 2% glucose, 22.4 mg/L uracil, and 80 mg/L tryptophan). To induce gametogenesis cells were transferred to conditioned sporulation media containing 2% potassium acetate, amino acid supplements and ampicillin (40 mg/L adenine, 40 mg/L uracil, 10 mg/L histidine, 10 mg/L leucine and 10 mg/L tryptophan, 100 µg/mL ampicillin) at an OD_{600} of 0.8. All meiotic cultures were incubated on a shaker for 24h at 30°C to complete gametogenesis. To increase efficiency of gametogenesis, conditioned sporulation media was obtained by filter sterilizing a meiotic culture at 1.85 OD_{600} after 5 hours at 30°C and was stored at 4°C. For immunoblotting saturated YPD 2% cultures were re-diluted to 0.2 OD_{600} in BYTA (1% yeast extract, 2% bacto tryptone, 1% potassium acetate, and 50mM potassium phthalate) containing acetate as a carbon source and then grown overnight to saturation at 30°C before transfer to unconditioned sporulation media without ampicillin at an OD_{600} of 1.85.

Fluorescent Microscopy

Bud scar staining and Pma2-GFP expression patterns during meiosis and gamete maturation were visualized using a DeltaVision Elite wide-field fluorescence microscope (GE Healthcare), equipped with a 60x/1.42 NA oil-immersion objective. Images were deconvolved with softWoRx imaging software (GE Healthcare). Time lapse images were acquired using a CellAsics system as previously described (King et al., 2019).

Replicative lifespan timelapse imaging was performed using an ECHO Revolution (RON-K) microscope equipped with an Olympus 40x/1.4 NA oil-immersion objective.

Age sorting of pre-gametogenic yeast cells

Young and aged cell populations were sorted by biotin-labeling of a founder population followed by bead-mediated magnetic sorting (Smeal et al., 1996). First, a patch of diploid cells was inoculated in YPD (2%) and grown overnight shaking at room temperature until saturation. Cells were then re-diluted in YPD (2%) to an OD_{600} of 0.2 and grown at 30°C to an OD_{600} of 0.6-1. To increase yield, 2 x 8 OD_{600} units were harvested per genotype, washed 3x with PBS (pH 8), and then were transferred into PBS (pH 8) containing 2 mg/mL EZ-Link Sulfo-NHS-LC-biotin (ThermoFisher Scientific). Cells were vortexed for one minute and incubated for 30 minutes at 4°C on a nutator, washed 4 times with PBS + glycine (pH 8 + 100 mM glycine), and then washed once with YPD 2% before being added to two separate 500 mL flasks containing 50 mL YPD 2% + ampicillin (100 µg/mL) each. Biotin labeled cultures were aged for 15-19h shaking at 30°C. Aged cell cultures were pelleted, washed once with 20 mL PBS (pH 7.4 + 0.5% BSA), and then resuspended in 20 mL PBS (pH 7.4 + 0.5%) BSA containing 100 µL of anti-biotin magnetic beads (Miltenyi Biotechnology). Cells were incubated for 15 min at 4°C and mixed regularly by inversion, washed once with 20 mL PBS (pH 7.4 + 0.5% BSA) and then resuspended in 5 mL PBS (pH 7.4 + 0.5% BSA). Using a QuadroMacs sorter, both suspensions were applied to a column each. The first flowthrough from each column was collected, combined, and used as the young cell population. Each column was washed 4 times with 3 mL PBS (pH 7.4 + 0.5% BSA) before eluting into a second column, to increase purity. The second columns were washed three times with 3 mL PBS (pH 7.4 + 0.5% BSA), cells were eluted, combined, and subsequently used as the aged cell population.

Immunostaining and gametogenesis

Young and aged cell suspensions were washed twice with 12 mL PBS (pH 7) and resuspended in 4 mL PBS (pH 7). 4 µL of Wheat Germ Agglutinin, Alexa 350 Fluor conjugate (1 µg/mL, ThermoFisher Scientific) and anti-streptavidin (564 nm) (1 µg/mL) was added respectively and incubated for 15 minutes in the dark at room temperature. Cells where washed (3x) with 12 mL of unconditioned sporulation media and resuspended to an OD_{600} of 0.8 in conditioned sporulation media + ampicillin (100 µg/mL). 0.1 OD_{600} units of cells was fixed in 3.7% formaldehyde to assess age before gametogenesis. Cultures were incubated for 24 hours at 30°C in the dark to complete gametogenesis and a 0.1 OD_{600} units of cells were used directly to count tetrad formation and another fraction of cells were fixed in 3.7% formaldehyde to assess age post-gametogenesis by imaging and counting biotinylated cells as well as bud scars.

Tetrad separation into single gametes and re-growth

Post gametogenic age sorted cultures were pelleted and resuspended in 900 µL H_2O, 100 µL Zymolase (1 mg/mL) and 2 µL B-mercaptoethanol and the suspension was incubated for 3 hours on a nutator at 30°C. Cells were washed (1x) with H_2O and resuspended in 1 mL H_2O followed by repeated sonication (6x 20 seconds) incubating the cells 2-3 minutes on ice in-between sonication cycles. Upon tetrad separation, separated gametes were filtered (30 µm Pre-separation filter, militenyibiotec) and diluted in YPD 2% + ampicillin (100 µg/mL) to an OD_{600}

of 0.8. After 3 hours at incubation on a nutator at 30°C, 1 mL of cell suspension was aliquoted, sonicated briefly for 5 seconds and filtered before loading into the microfluidics system.

Microfluidics loading and timelapse imaging of replicative lifespan

Microfluidics devices (**Fig S1** adapted from (Jo et al., 2015);18++ chips from iBiochips) were setup using the manufacturer's recommendations on an ECHO Revolution fluorescence microscope in the inverted position with the environmental chamber set to 30˚C. Briefly, 20 mL syringes (Becton, Dickinson and Company) were filled with ~15 mL of YPD 2% + ampicillin (100 µg/mL) + 1% Pluronic F-127 (P2443, Sigma), and then connected to a Clay Adams Intramedic Luer-Stub Adapter (Becton, Dickinson and Company). Non-DEHP Medical Grade Tubing (iBiochips, MTB-100, ID = 0.202", OD = 0.060", wall = 0.20") equipped with a hollow stainless-steel pin (iBiochips, HSP-200) was then used to connect the media syringe to the imaging units using the "media loading" ports. "Cell loading" ports were plugged with solid stainless-steel pins (iBiochips, SSP-200) while imaging units were primed with media for at least 2 hours with a flow rate of 2.4 µL/min using micropumps (iBiochips,78-7200BIO). After all units were filled with media, pumps were stopped an hour prior to cell loading. For cell loading, 5 mL syringes (Becton, Dickinson and Company) with Clay Adams Intramedic Luer-Stub Adapter (Becton, Dickinson and Company) were filled with 1 mL of cells diluted to an OD_{600} of 0.8 in YPD 2% + ampicillin (100 µg/mL). Solid stainless-steel pins were then removed from the "cell loading" ports and tubing and open stainless-steel pins were used to connect the syringe containing cells with the microfluidic device. Cells were loaded manually and, once sufficient cells were loaded, the "cell loading" ports were plugged with solid stainless-steel pins and media flow was resumed at 2.4 µL/min.

Timelapse imaging was performed using an Olympus 40x/1.4 NA oil-immersion objective with intervals of 15-20 minutes for 72 hours. The x-, y-, and z-motors were set to medium speed; however, varying stage speeds caused sporadic differences in imaging intervals. Thus, the recorded acquisition time provides accurate timing information. For each chamber, 2x27 images and three z-slices per position with 3-5 µm spacing, to compensate for focal plane differences across a single unit, were acquired. Autofocus was set across a 20 µm range with 0.2 µm spacing using the "Course-Fine" setting (Threshold = 4, Contrast Limit = 4). The XY Stage and Z Motor were both set to medium speed and Hyperscan was enabled for the "BF" channel using "Y-Axis" Axis Priority and "Bi" Scanning Pattern.

Quantification of replicative age and purity of sorted cells

Z-stacks (36 slices, 0.2 µm spacing) of fixed young and aged cells/tetrads were acquired on a DeltaVision Elite wide-field fluorescence microscope (GE Healthcare), using a 60x/1.42 NA oil-immersion objective and deconvolved with softWoRx imaging software (GE Healthcare). To reliably count number of bud scars, images were cropped, 3D projected and counted using a custom semi-automated FIJI script (ImageJ2, V. 2.14.0/1.54m, (Schindelin et al., 2012)). Max intensity Z-projections were generated and displayed as examples in figures.

Quantification of gamete replicative lifespan

After the movie was completed, the ECHO batch exporter tool was used to export stitched TIFF images. Individual TIFF images were converted to 8-bit using FIJI (ImageJ2, V.

2.14.0/1.54m, (Schindelin et al., 2012)), then full chamber time-lapse could be opened using the "Bio Formats Import" tool with the "Group files with similar names" box checked. Single Pma2-GFP positive cells (gametes) were identified by eye and cropped both in the FITC image and the brightfield time course using a custom semi-automated FIJI script. Next using a semi-automated FIJI script, the replicative lifespan of Pma2-GFP positive cells (gametes) identified in the FITC image were counted, verifying identity by comparing the FITC and brightfield time-lapse for each single gamete. If a cell ejected from the U-trap before senescence was observed, this was noted and treated as a censored subject for quantification. For most experiments, counts from two technical replicates were concatenated unless otherwise indicated. Although throughput to quantify gametogenic reset of lifespan is significantly higher than with previous methods, cell divisions of each gamete must still be counted manually by a trained scientist rendering data analysis as a current bottleneck of the presented method.

Immunoblotting

For each sample, 4-10 OD_{600} units were harvested and pelleted from either log-phase YPD 2%, saturated YPD 2%, saturated BYTA or indicated timepoints upon transfer to sporulation media. For each sample, 2 mL 5% trichloroacetic acid was added and cells were incubated for ≥10 minutes at 4°C minutes, washed (1x) with acetone, and pellets was dried overnight. For protein extraction, ~100 µL glass beads and 100 µL of lysis buffer (50 mM Tris-HCl pH 8.0, 1 mM EDTA, 3 mM DTT, 2.2 mM PMSF, 1x complete EDTA-free inhibitor cocktail (Roche)) were added to the dried pellets and transferred to a Mini-Beadbeater-96 (BioSpec) for 5 minutes. Fifty µL of 3X SDS sample buffer (187.5 mM Tris pH 6.8, 6% β-mercaptoethanol, 30% glycerol, 9% SDS, 0.05% bromophenol blue) was added and samples were for boiled for 5 minutes at 95°C. Polyacrylamide gel electrophoresis (4–12% Bis-Tris Bolt gels, Thermo Fisher) and semi-dry transfer (Trans-Blot Turbo Transfer System, Bio-Rad) onto nitrocellulose membranes apparatus was used to separate and visualize proteins respectively. Odyssey PBS Blocking Buffer (LI-COR Biosciences) was used to block membranes (90 minutes, room temperature), and membranes were incubated overnight at 4°C with a mouse anti-3v5 (R960-25; RRID: AB_2556564, Thermo Fisher) antibody at 1:2000 in PBS +0.1% Tween-20 and a rabbit anti-Hx2k (RRID:AB_219918, 100–4159, Rockland) at 1:20000 in PBS +0.1% tween. Membranes were washed with PBS+ 0.1% Tween-20 (4x, 5 minutes each) and incubated with secondary antibody solutions containing anti-mouse conjugated to IRDye 800CW at a 1:15,000 dilution (RRID:AB_621847, 926–32212, LI-COR Biosciences) and an anti-rabbit conjugated to IRDye 680RD at a 1:15,000 dilution (RRID:AB_10956166, 926–68071, LI-COR Biosciences) in PBS +0.1% Tween-20. Membranes were imaged using an Odyssey CLx system (LI-COR Biosciences).

Statistical analysis

Prism Graphpad (version 10.1.0) was used to plot and analyze data. Prism Graphpad was used to calculated mean and standard deviation of replicative ages and to assess statistical significance in differences between replicative lifespans using the Log-rank (Mantel-cox) test. A Python script was used to calculated 95% confidence intervals using the Wilson score method.

Acknowledgements

We thank the current and former members of the Brar and Ünal laboratory for critical discussion and comments on the manuscript. This work is supported by the Swiss National Science Foundation mobility fellowship P500PB_214421 to S.S., G.B. is supported by funding from the National Institutes of Health (R01AG071869) and the Astera Fund, TLS was supported by a Longevity Impetus Grant from the Norn Group, Hevolution Foundation and Rosenkranz Foundation. E.Ü. is supported by funding from the National Institutes of Health (R01AG071801) and the Astera Institute.

Author contributions

S.S. and N.P. performed experiments, S.S. and N.P. analyzed the data, S.S., T.L.S., N.P., J.S.G., E.Ü., G.A.B., wrote and edited the manuscript.

Declaration of interests:

The authors declare no competing interests.

Figures & Figure Legends

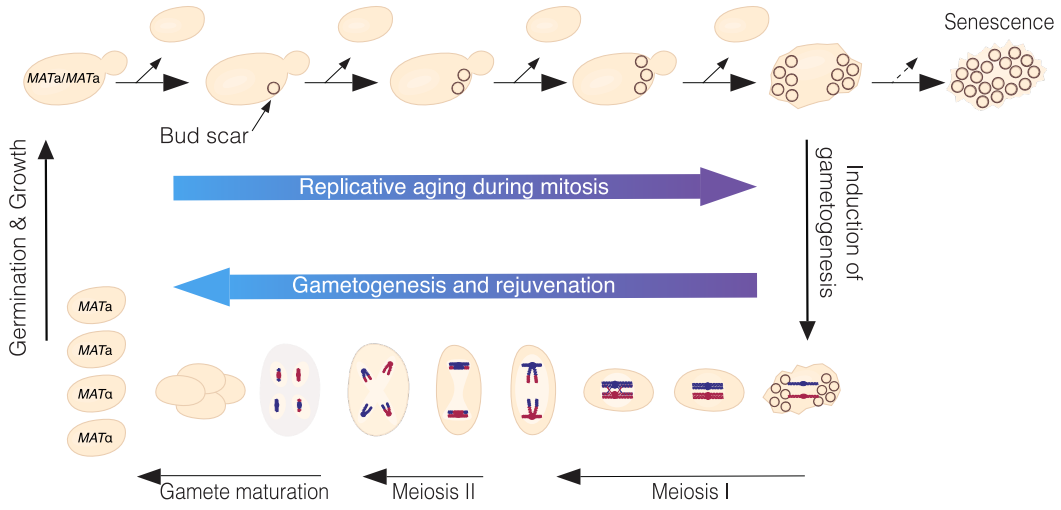

Figure 1. Replicative lifecycle and gametogenic rejuvenation in *Saccharomyces cerevisiae*. In vegetative growth, yeast cells divide asymmetrically, with the daughter cell born young while the mother cell accumulates aged and damaged components until reaching senescence. Replicative age of a single yeast cell is determined by the number of bud scars, which form at each division and are retained on the cell wall (top panel). Gametogenesis can be induced by nutrient depletion (downwards arrow, right). During gametogenesis, diploid yeast divides symmetrically, fully resetting their lifespan and leading to the formation of four equally young haploid gametes with two different matting types, even from aged precursor cells (bottom panel). Addition of nutrients induces germination and return to mitotic growth (upward arrow, left).

Figure 2

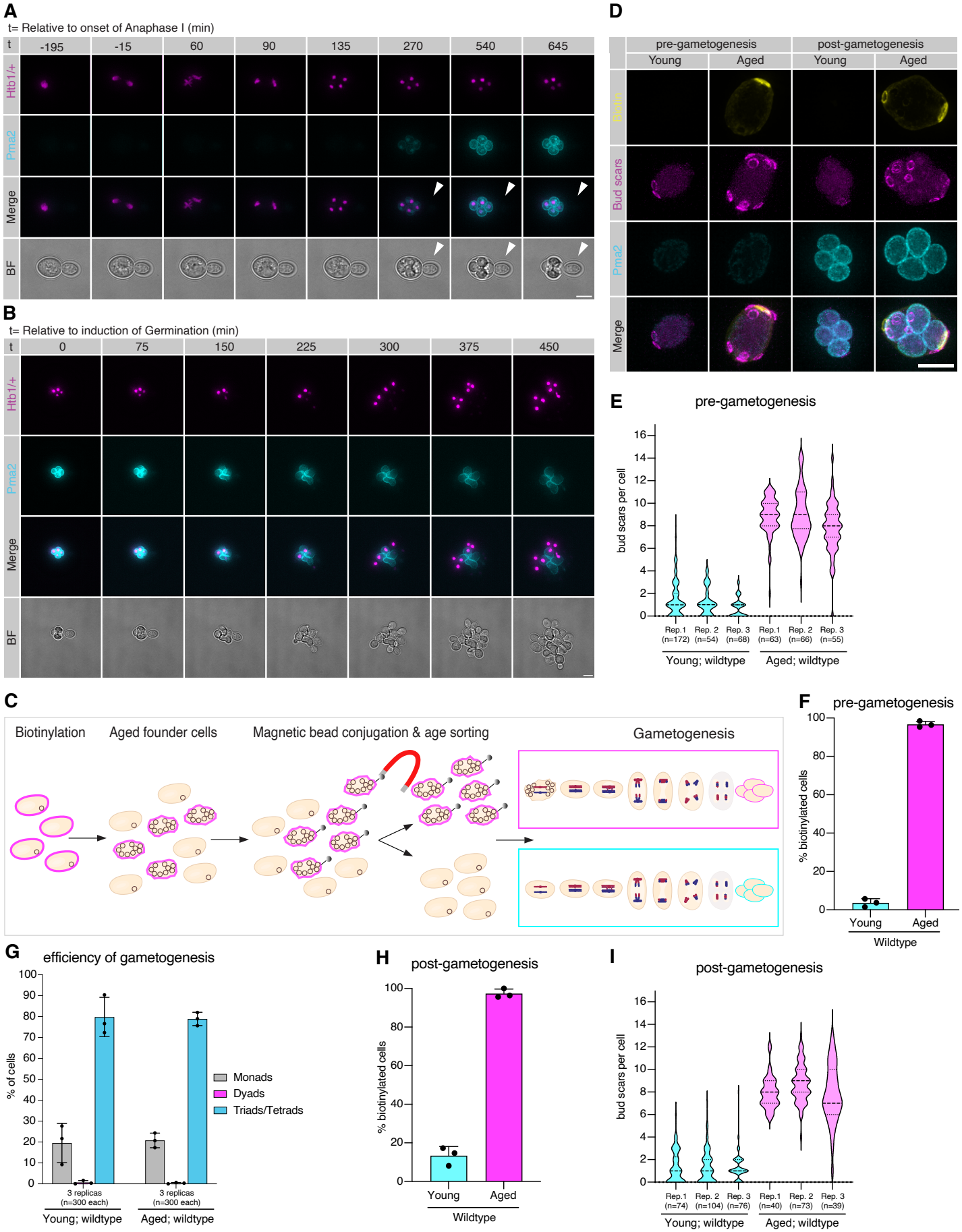
A
t= Relative to onset of Anaphase I (min)
t
-195
-15
60
90
135
270
540
645
Htb1/+
Pma2
Merge
BF
B
t= Relative to induction of Germination (min)
0
75
150
225
300
375
450
C
Biotinylation
Aged founder cells
Magnetic bead conjugation & age sorting
Gametogenesis
D
pre-gametogenesis
post-gametogenesis
Young
Aged
Bid1h
Bud scars
E
pre-gametogenesis
bud scars per cell
Rep.1 (n=172)
Rep. 2 (n=54)
Rep. 3 (n=68)
Rep.1 (n=63)
Rep. 2 (n=66)
Rep. 3 (n=55)
Young; wildtype
Aged; wildtype
F
pre-gametogenesis
% biotinylated cells
Young
Aged
Wildtype
G
efficiency of gametogenesis
% of cells
Monads
Dyads
Triads/Tetrads
3 replicas (n=300 each)
Young; wildtype
Aged; wildtype
H
post-gametogenesis
% biotinylated cells
Young
Aged
Wildtype
I
post-gametogenesis
bud scars per cell
Rep.1 (n=74)
Rep. 2 (n=104)
Rep. 3 (n=76)
Rep.1 (n=40)
Rep. 2 (n=73)
Rep. 3 (n=39)
Young; wildtype
Aged; wildtype

Figure 2. Gametogenesis-specific expression of Pma2 remains detectable post-germination in age-sorted gametes

(**A**) Montage of max-intensity projected diploid cell progressing through gametogenesis visualizing Pma2-GFP (cyan) and a Htb1-mCherry (magenta) marking histones.

(**B**) Montage of a germinating max-intensity projected tetrad visualizing Pma2-GFP (cyan) and a Htb1-mCherry (magenta) marking histones.

(**C**) Schematic depiction of age sorting by biotin mediated magnetic bead conjugation.

(**D**) Representative age sorted pre-gametogenic max-intensity projected cells (left panel) and post-gametogenic tetrads (right panel) visualizing biotin label (yellow), chitin rich bud scars (magenta) and Pma2-GFP (cyan).

(**E**) Quantification of replicative age by assessing number of bud scars in young (1.16 ± 0.41, mean ± SD, n=3 replicas, n=172; 54 and 68 respectively) and aged (8.55 ± 0.66 (mean ± SD, 3 replicas, n=63, 66 and 55 respectively) wildtype cell populations.

(**F**) Quantification of fraction of biotinylated cells in young (3.63 ± 2.12 %, mean ± SD, 3 replicas, n=175, 54 and 68 respectively) and aged (96.74 ± 1.58 %, mean ± SD, 3 replicas, n=65, 66 and 55 respectively) wildtype cell populations.

(**G**) Quantification of fraction of tetrads in young (79.8 ± 9.43%; mean ± SD, 3 replicas n=300 each) and aged (aged: 78.89 ± 3.17 %, mean ± SD, 3 replicas n=300 each) post gametogenic wildtype cell populations.

(**H**) Quantification of fraction of biotinylated tetrads in young (13.38 ± 4.74%, mean ± SD, n=3 replicas, n=74, 104 and 76 respectively) and aged (97.34 ± 2.33%, mean ± SD, 3 replicas, n=46, 73 and 39 respectively) wildtype populations after completion of gametogenesis.

(**I**) Quantification of replicative age by assessing number of bud scars in young (1.31 ± 0.04, mean ± SD, 3 replicas, n=74, 104 and 76 respectively) and aged (8.17 ± 0.54, mean ± SD, 3 replicas, n=40, 73 and 39 respectively) wildtype tetrad populations.

Scale bars are 5 µm and confidence intervals were calculated using the Wilson score method.

Figure 3

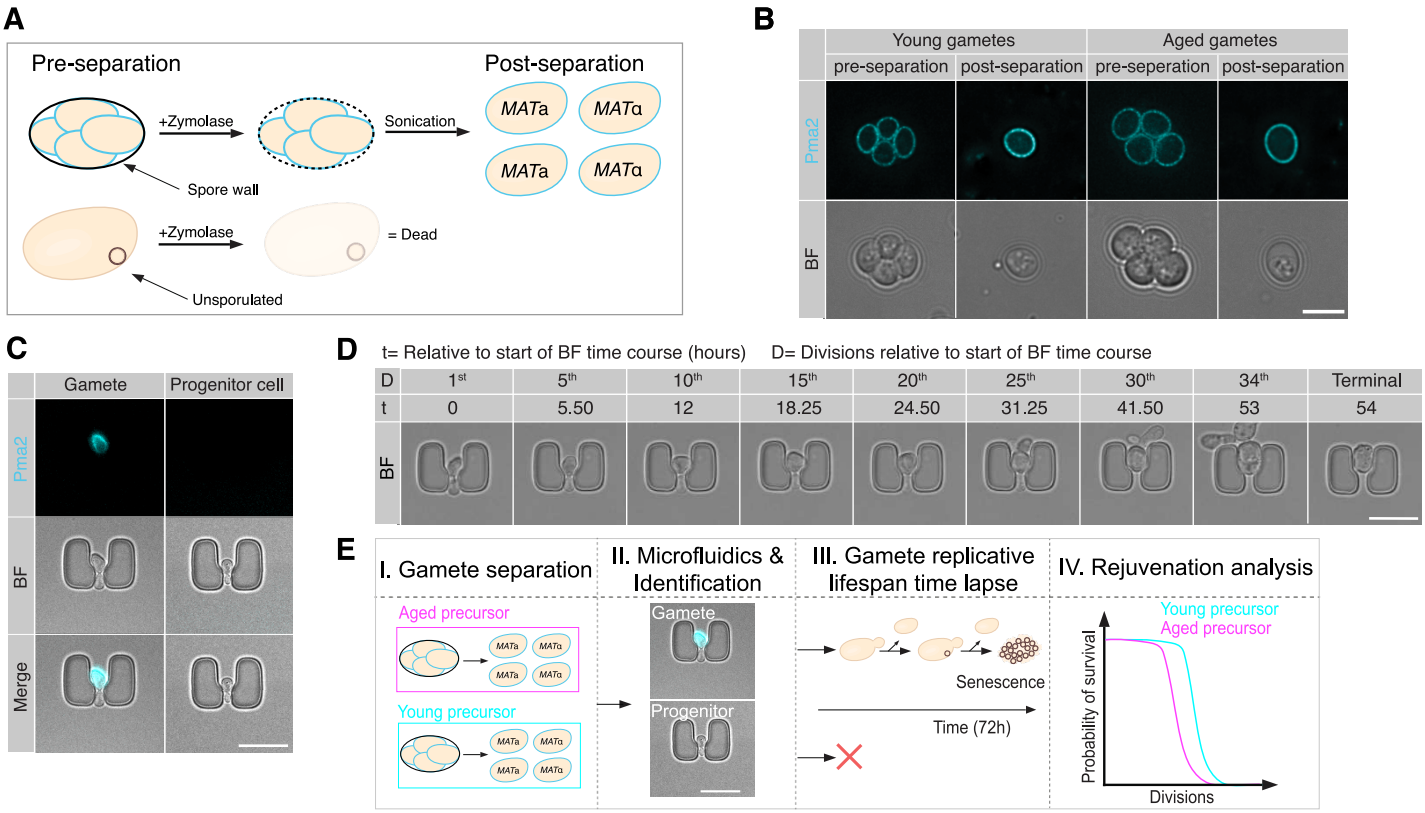

Figure 3. Separation of tetrads into single sterile gametes to assess gamete replicative lifespan with microfluidics

(**A**) Schematic depiction of tetrad separation procedure.

(**B**) Representative single z-slices of pre- and post-separated young (left panel) and old (right panel) tetrads and gametes, respectively, visualizing brightfield and Pma2-GFP (cyan).

(**C**) Representative Pma2-GFP positive gamete (left panel) and Pma2-GFP negative gamete progenitor (right panel) trapped in microfluidics-based devices visualizing brightfield and Pma2-GFP (cyan).

(**D**) Representative trapped gamete visualizing every 5th division until the terminal 34th division over the time of 54 hours.

(**E**) Schematic depiction of the developed pipeline to assess gametes replicative lifespan.

Scale bars are 5 µm.

Figure 4

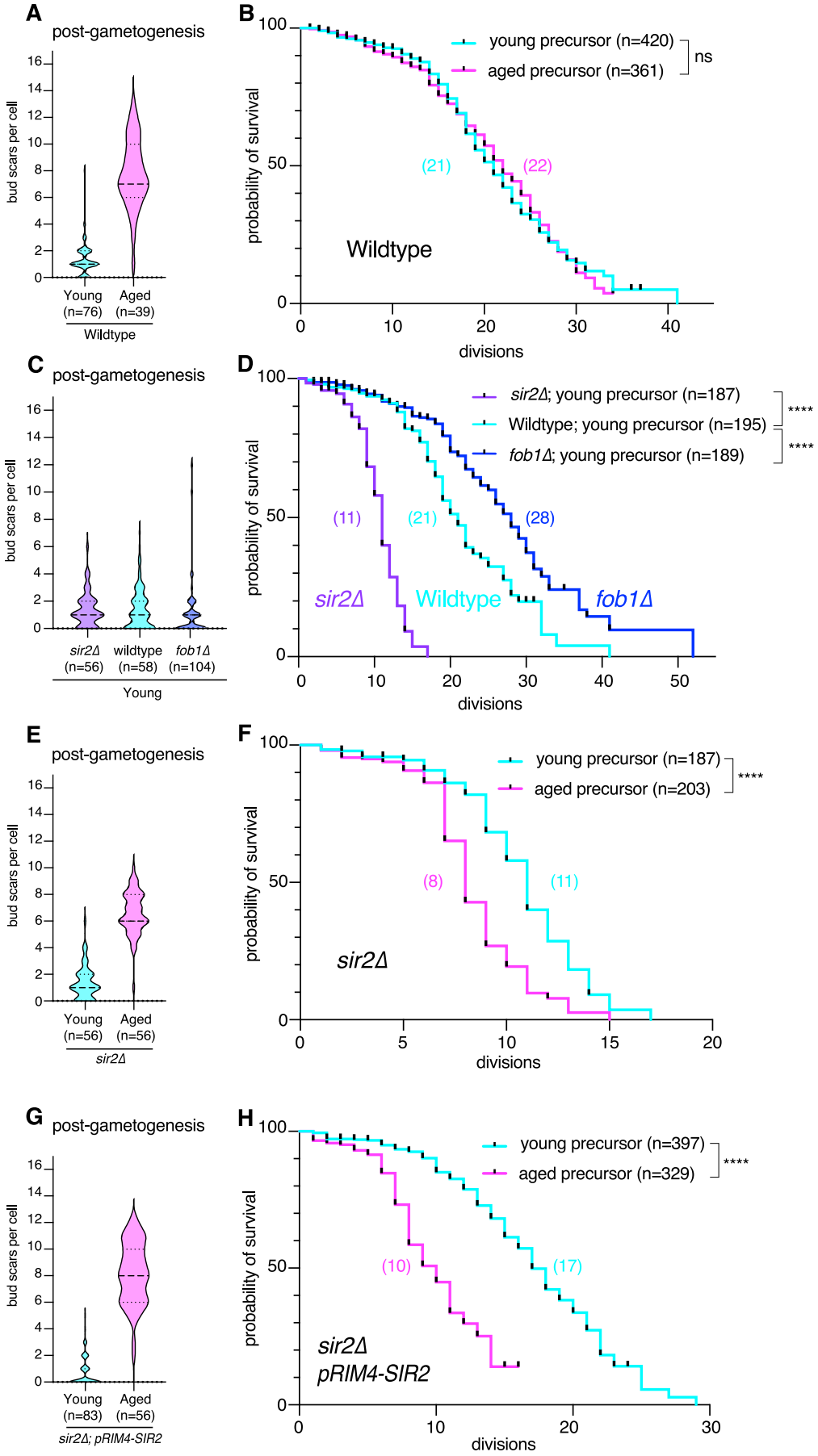
A
post-gametogenesis
bud scars per cell
Young (n=76)
Aged (n=39)
Wildtype
B
young precursor (n=420)
aged precursor (n=361)
ns
(21)
(22)
Wildtype
probability of survival
divisions
C
post-gametogenesis
sir2Δ (n=56)
wildtype (n=58)
fob1Δ (n=104)
Young
D
sir2Δ; young precursor (n=187)
Wildtype; young precursor (n=195)
fob1Δ; young precursor (n=189)
****
****
(11)
(21)
(28)
sir2Δ
Wildtype
fob1Δ
E
post-gametogenesis
Young (n=56)
Aged (n=56)
sir2Δ
F
young precursor (n=187)
aged precursor (n=203)
****
(8)
(11)
sir2Δ
G
post-gametogenesis
Young (n=83)
Aged (n=56)
sir2Δ; pRIM4-SIR2
H
young precursor (n=397)
aged precursor (n=329)
****
(10)
(17)
sir2Δ
pRIM4-SIR2

Figure 4. Replicative lifespan resets in wildtype gametes but rejuvenation fails in *sir2*Δ mutants through a gametogenesis-independent mechanism.

(**A**) Quantification of replicative age by assessing number of bud scars in young (1.3± 1.2, mean ± SD, n=76) and aged (7.8± 2.6, mean ± SD, n=39) wildtype gamete populations.
(**B**) Quantification of replicative lifespan of young (median lifespan=21, n=420, 223 censored subjects) and aged (median lifespan=22, n=361, 213 censored subjects, p=0.982 compared to young) wildtype gametes.
(**C**) Quantification of replicative age by assessing number of bud scars in young *sir2*Δ (1.3± 1.3, mean ± SD, n=56), wildtype (1.4± 1.5, mean ± SD, n=104) and *fob1*Δ (11.2± 2.2, mean ± SD, n=53) gamete populations.
(**D**) Quantification of replicative lifespan of young *sir2*Δ (median lifespan=11, n=187, 80 censored subjects, p<0.0001 compared to wildtype), wildtype (median lifespan=21, n=195, 103 censored subjects) and *fob1*Δ (median lifespan=28, n=286, 174 censored subjects, p<0.0001 compared to wildtype) gametes.
(**E**) Quantification of replicative age by assessing number of bud scars in young (1.3± 1.3, mean ± SD, n=56, same data as shown in Fig. 4D) and aged (6.6± 1.6, mean ± SD, n=56) *sir2*Δ gamete populations.
(**F**) Quantification of replicative lifespan of young (median lifespan=11, n=187, 80 censored subjects, same data as shown in Fig. 3F) and aged *sir2*Δ (median lifespan=8, n=203, 103 censored subjects, p<0.0001 compared to young) gametes.
(**G**) Quantification of replicative age by assessing number of bud scars in young (0.72± 1.1, mean ± SD, n=83) and aged 8.1 ± 2.3 (mean ± SD, n=56) *pRIM4-SIR2 sir2*Δ gamete populations.
(**H**) Quantification of replicative lifespan of young (median lifespan17, n=397, 266 censored subjects) and aged *pRIM4-SIR2 sir2*Δ (median lifespan=10 (n=329, 219 censored subjects, p<0.0001 compared to young) gametes.
Confidence intervals were calculated using the Wilson score method and statistical significance for differences between replicative lifespans was calculated using the Log-rank (Mantel-cox) test, tick marks on survival curves represent censored events.

Figure 5

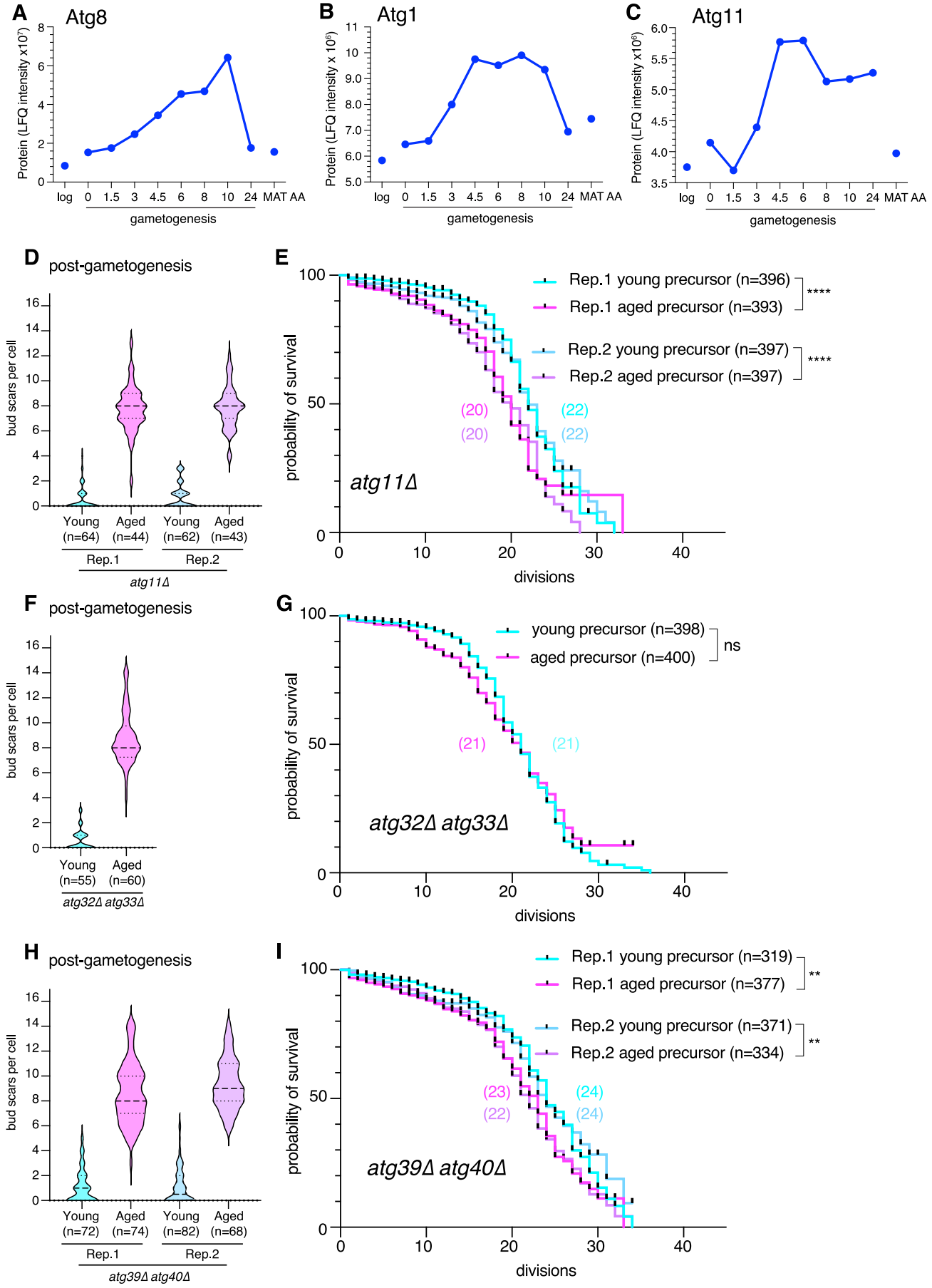
A
Atg8
Protein (LFQ intensity x10^7)
log 0 1.5 3 4.5 6 8 10 24 MAT AA
gametogenesis
B
Atg1
Protein (LFQ intensity x 10^6)
log 0 1.5 3 4.5 6 8 10 24 MAT AA
gametogenesis
C
Atg11
Protein (LFQ intensity x10^6)
log 0 1.5 3 4.5 6 8 10 24 MAT AA
gametogenesis
D
post-gametogenesis
bud scars per cell
Young (n=64)
Aged (n=44)
Young (n=62)
Aged (n=43)
Rep.1
Rep.2
atg11Δ
E
probability of survival
Rep.1 young precursor (n=396)
Rep.1 aged precursor (n=393)
****
Rep.2 young precursor (n=397)
Rep.2 aged precursor (n=397)
****
(20)
(20)
(22)
(22)
atg11Δ
divisions
F
post-gametogenesis
bud scars per cell
Young (n=55)
Aged (n=60)
atg32Δ atg33Δ
G
probability of survival
young precursor (n=398)
aged precursor (n=400)
ns
(21)
(21)
atg32Δ atg33Δ
divisions
H
post-gametogenesis
bud scars per cell
Young (n=72)
Aged (n=74)
Young (n=82)
Aged (n=68)
Rep.1
Rep.2
atg39Δ atg40Δ
I
probability of survival
Rep.1 young precursor (n=319)
Rep.1 aged precursor (n=377)
**
Rep.2 young precursor (n=371)
Rep.2 aged precursor (n=334)
**
(23)
(22)
(24)
(24)
atg39Δ atg40Δ
divisions

Figure 5. Selective autophagy of the ER but not the mitochondria is necessary to reset replicative lifespan during gametogenesis.

(**A-C**) Protein levels (mass spectrometry) of autophagy factors either during log-phase vegetative growth in 2% glucose containing media (log), the indicated time in gametogenesis inducing media (h), or in control diploids that cannot undergo gametogenesis (*MAT*a/a) plotted from previously generated meiotic datasets (Cheng et al., 2018).
(**A**) Atg8 protein levels (mass spectrometry).
(**B**) Atg1 protein levels (mass spectrometry).
(**C**) Atg11 protein levels (mass spectrometry).
(**D**) Quantification of replicative age by assessing number of bud scars in *atg11*Δ tetrad populations: Rep. 1 young (0.53± 0.31, mean ± SD, n=64) and aged of (7.8± 1.8, mean ± SD, n=44); Rep. 2 young (0.82± 1, mean ± SD, n=62) and aged of (7.9± 1.7, mean ± SD, n=43).
(**E**) Quantification of replicative lifespan of *atg11*Δ gametes: Rep.1 young (median lifespan=22, n=393, 267 censored subjects) and aged (median lifespan=20, n=396, 255 censored subjects, p>0.0001); Rep. 2 young (median lifespan=20, n=397, 280 censored subjects) and aged (median lifespan=22, n=397, 259 censored subjects, p>0.0001compared to young).
(**F**) Quantification of replicative age by assessing number of bud scars in young (0.6± 0.85, mean ± SD, n=55), and aged (8.8± 2.1, mean ± SD, n=60) *atg32*Δ *atg33*Δ gamete populations.
(**G**) Quantification of replicative lifespan of young (median lifespan=21, n=398, 154 censored subjects) and aged *atg32*Δ *atg33*Δ double mutants (median lifespan=21, n=400, 192 censored subjects, p=0.7414 compared to young) gametes.
(**H**) Quantification of replicative age by assessing number of bud scars in *atg39*Δ *atg40*Δ tetrad populations: Rep. 1 young (1.1± 1.4, mean ± SD, n=72) and aged of (8.6± 2.5, mean ± SD, n=74); Rep. 2 young (1.1± 1.5, mean ± SD, n=82) and aged of (9.4± 2, mean ± SD, n=68).
(**I**) Quantification of replicative lifespan of *atg39*Δ *atg40*Δ gametes: Rep.1 young (median lifespan=24, n=319, 195 censored subjects) and aged (median lifespan=23, n=377, 238 censored subjects, p=0.0030 compared to young); Rep. 2 young (median lifespan=24, n=371, 240 censored subjects) and aged (median lifespan=22, n=334, 219 censored subjects, p=0.0080 compared to young).
Statistical significance for differences between replicative lifespans was calculated using the Log-rank (Mantel-cox) test, tick marks on survival curves represent censored events.

Figure 6

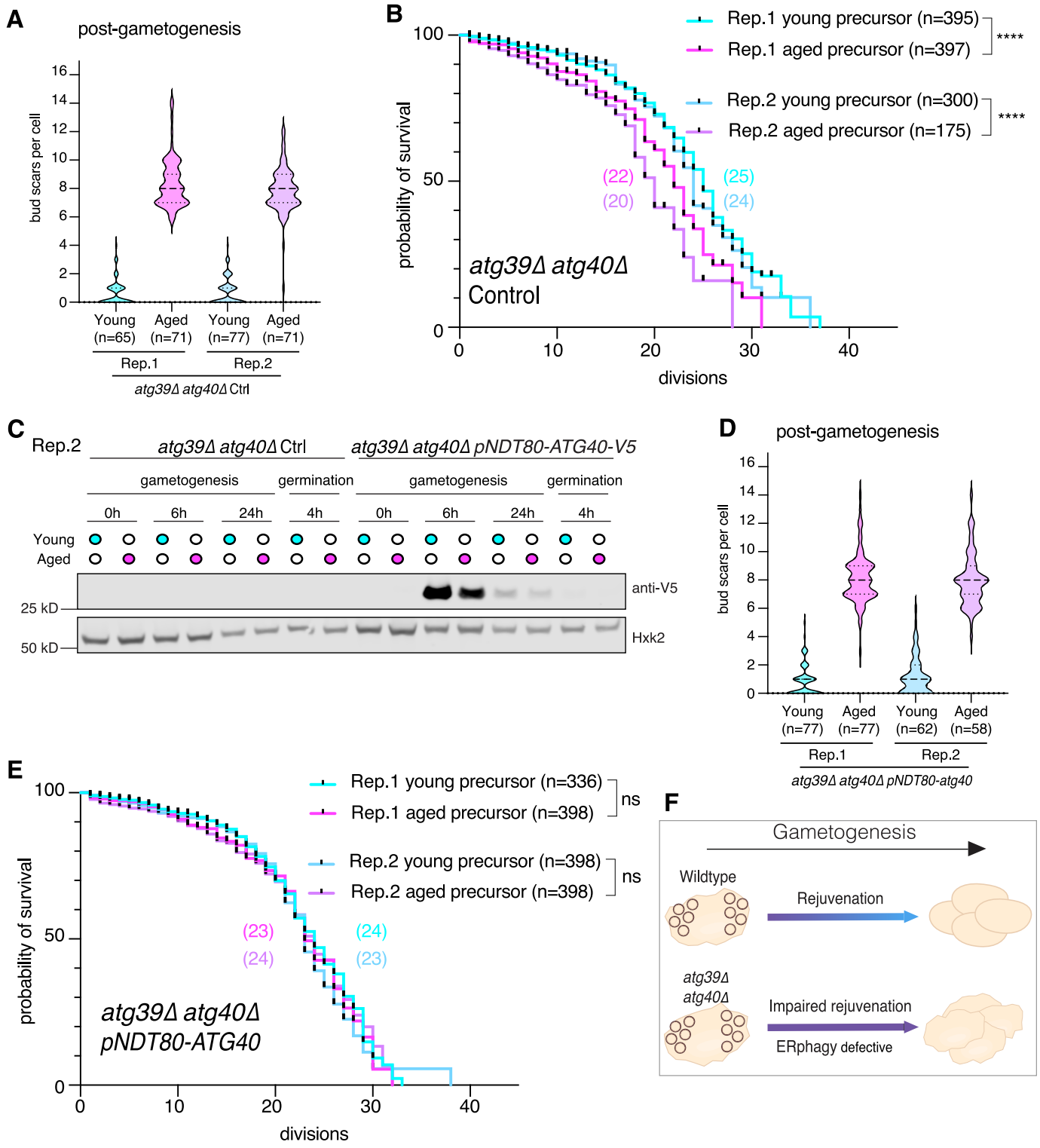
A
post-gametogenesis
bud scars per cell
Young (n=65)
Aged (n=71)
Young (n=77)
Aged (n=71)
Rep.1
Rep.2
atg39Δ atg40Δ Ctrl
B
Rep.1 young precursor (n=395)
Rep.1 aged precursor (n=397)
****
Rep.2 young precursor (n=300)
Rep.2 aged precursor (n=175)
****
(22)
(20)
(25)
(24)
atg39Δ atg40Δ
Control
probability of survival
divisions
C
Rep.2
atg39Δ atg40Δ Ctrl
atg39Δ atg40Δ pNDT80-ATG40-V5
gametogenesis
germination
0h
6h
24h
4h
Young
Aged
anti-V5
Hxk2
25 kD
50 kD
D
post-gametogenesis
bud scars per cell
Young (n=77)
Aged (n=77)
Young (n=62)
Aged (n=58)
Rep.1
Rep.2
atg39Δ atg40Δ pNDT80-atg40
E
Rep.1 young precursor (n=336)
Rep.1 aged precursor (n=398)
ns
Rep.2 young precursor (n=398)
Rep.2 aged precursor (n=398)
ns
(23)
(24)
(24)
(23)
atg39Δ atg40Δ
pNDT80-ATG40
probability of survival
divisions
F
Gametogenesis
Wildtype
Rejuvenation
atg39Δ
atg40Δ
Impaired rejuvenation
ERphagy defective

Figure 6. Expression of *ATG40* during gametogenesis is sufficient to rescue replicative lifespan resetting in cells that lack ERphagy receptors.

(**A**) Quantification of replicative age by assessing number of bud scars in *atg39*Δ *atg40*Δ control tetrad populations: Rep. 1 young (0.62± 0.92, mean ± SD, n=65) and aged of (8.4± 1.7, mean ± SD, n=71); Rep. 2 young (0.74± 0.97, mean ± SD, n=77) and aged of (7.8± 1.6, mean ± SD, n=71).

(**B**) Quantification of replicative lifespan of *atg39*Δ *atg40*Δ control gametes: Rep.1 young (median lifespan=25, n=397, 229 censored subjects,) and aged (median lifespan=22, n=395, 277 censored subjects, p<0.0001compared to young); Rep. 2 young (median lifespan=24, n=300, 185 censored subjects, 1 technical replicate) and aged (median lifespan=20, n=175, 122 censored subjects, 1 technical replicate, p<0.0001 compared to young).

(**C**) Immunoblot of young and aged control and pNDT80-Atg40-V5 samples to quantify protein levels (anti-V5) and loading control (Hxk2) at different timepoints upon transfer to gametogenesis-inducing media (gametogenesis) and after re-growth in media containing 2% glucose (germination) (samples collected from Rep.2).

(**D**) Quantification of replicative age by assessing number of bud scars in *atg39*Δ *atg40*Δ *pNDT80-ATG40* tetrad populations: Rep. 1 young (0.87± 1.1, mean ± SD, n=77) and aged (8.1± 1.8, mean ± SD, n=77); Rep. 2 young (1.2± 1.47, mean ± SD, n=62) and aged (8.0± 1.9, mean ± SD, n=58).

(**E**) Quantification of replicative lifespan of *atg39*Δ *atg40*Δ *pNDT80-ATG40* gametes: Rep.1 young (median lifespan=24, n=398, 231 censored subjects) and aged (median lifespan=23, n=336, 242 censored subjects, one technical replica, p<0.4519 compared to young); Rep. 2 young (median lifespan=23, n=398, 256 censored subjects) and aged (median lifespan=24, n=398, 281 censored subjects, p=0.9538 compared to young).

(**F**) Schematic depiction of impaired gametogenic rejuvenation in ERphagy mutants.

Statistical significance for differences between replicative lifespans was calculated using the Log-rank (Mantel-cox) test, tick marks on survival curves represent censored events.

Supplementary Figures & Figure Legends

Figure S1

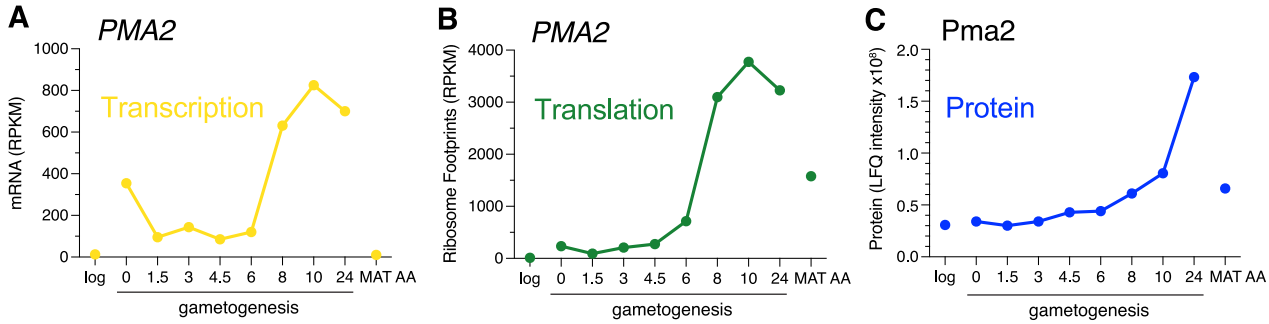

Figure S1. *PMA2* translation and protein levels are upregulated during late gametogenesis.

Expression of *PMA2* either during log-phase vegetative growth in 2% glucose containing media (log), the indicated time in gametogenesis inducing media (h), or in control diploids that cannot undergo gametogenesis (*MAT*a/a) plotted from previously generated meiotic datasets (Cheng et al., 2018).

(**A**) *PMA2* transcript levels (RNA-seq).

(**B**) *PMA2* translation levels (ribosome-protected footprints).

(**C**) Pma2 protein levels (mass spectrometry).

Figure S2

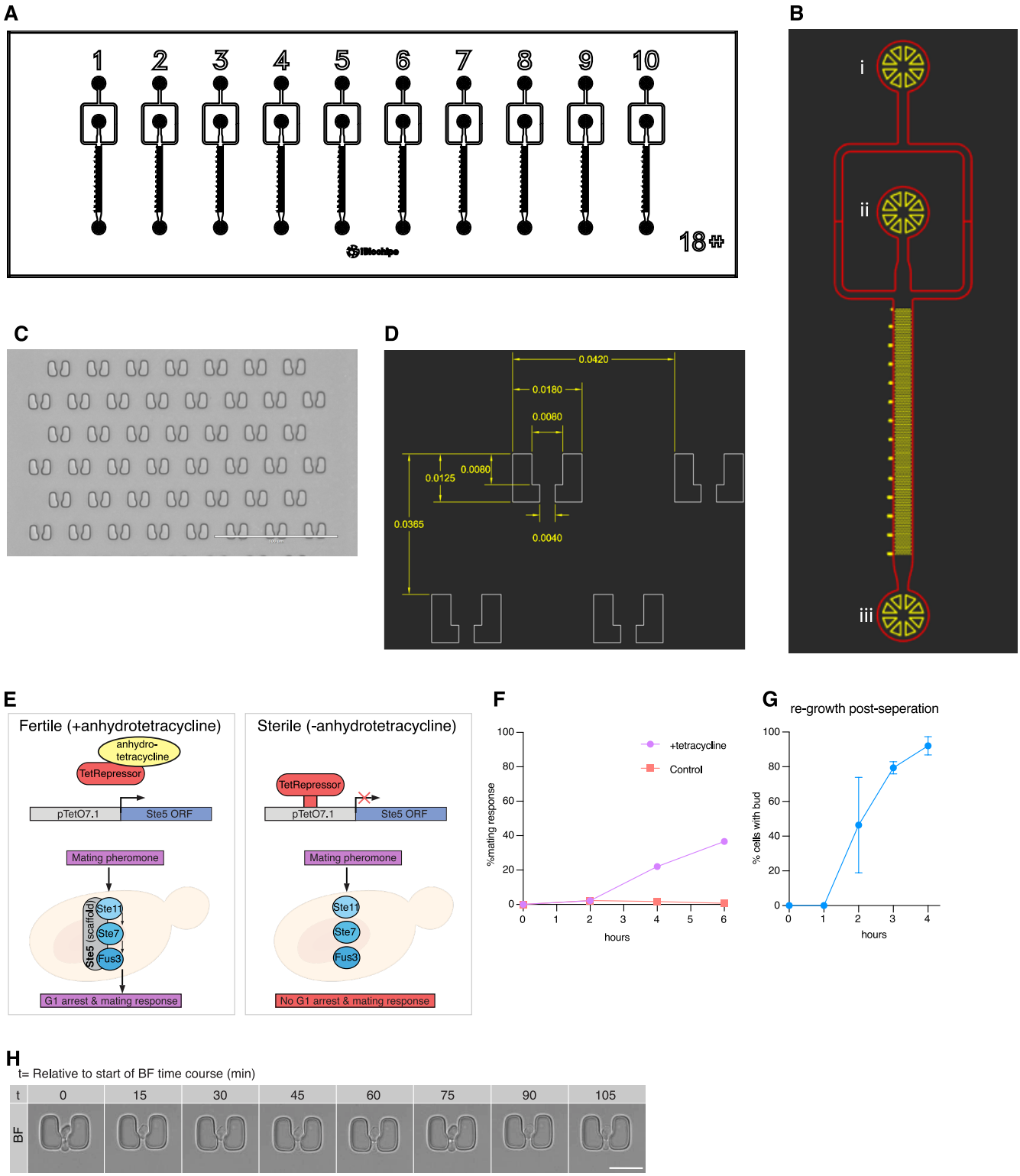
A
1
2
3
4
5
6
7
8
9
10
18#
B
i
ii
iii
C
D
0.0420
0.0180
0.0080
0.0125
0.0080
0.0365
0.0040
E
Fertile (+anhydrotetracycline)
anhydro-tetracycline
TetRepressor
pTetO7.1
Ste5 ORF
Mating pheromone
Ste5 (scaffold)
Ste11
Ste7
Fus3
G1 arrest & mating response
Sterile (-anhydrotetracycline)
TetRepressor
pTetO7.1
Ste5 ORF
Mating pheromone
Ste11
Ste7
Fus3
No G1 arrest & mating response
F
+tetracycline
Control
%mating response
hours
G
re-growth post-seperation
% cells with bud
hours
H
t= Relative to start of BF time course (min)
t
0
15
30
45
60
75
90
105
BF

Figure S2. Custom-built U-trap microfluidic devices with specific dimensions for vegetatively growing haploid SK1 cells.

(**A**) Schematic view of one microfluidic device with 10 separate imaging units.

(**B**) Schematic overview of one unit with (i) media inlet; cell loading inlet (ii) and waste outlet (iii). During the experiment media flows from media inlet (i) to waste outlet (iii) while cell loading inlet is plugged with a solid stainless-steel pin.

(**C**) Image of U-traps and spacing in one unit, scale bar is 100 µm.

(**D**) Custom developed SK1 specific dimensions of trap width and height (8 µm), exit channel width (4 µm), and spacing between traps (24 µm).

(**E**) Schematic depiction of genetic system to achieve constitutive sterility.

(**F**) Quantification of mating response scoring hybrid formation upon 1:1 mixing of *MAT*a and *MAT*α cells.

(**G**) Monitoring of re-growth of separated gametes in glucose containing liquid culture by scoring emergence of buds.

(**H**) Representative trapped gamete dividing twice over the time of two hours, scale bar is 5 µm.

Figure S3

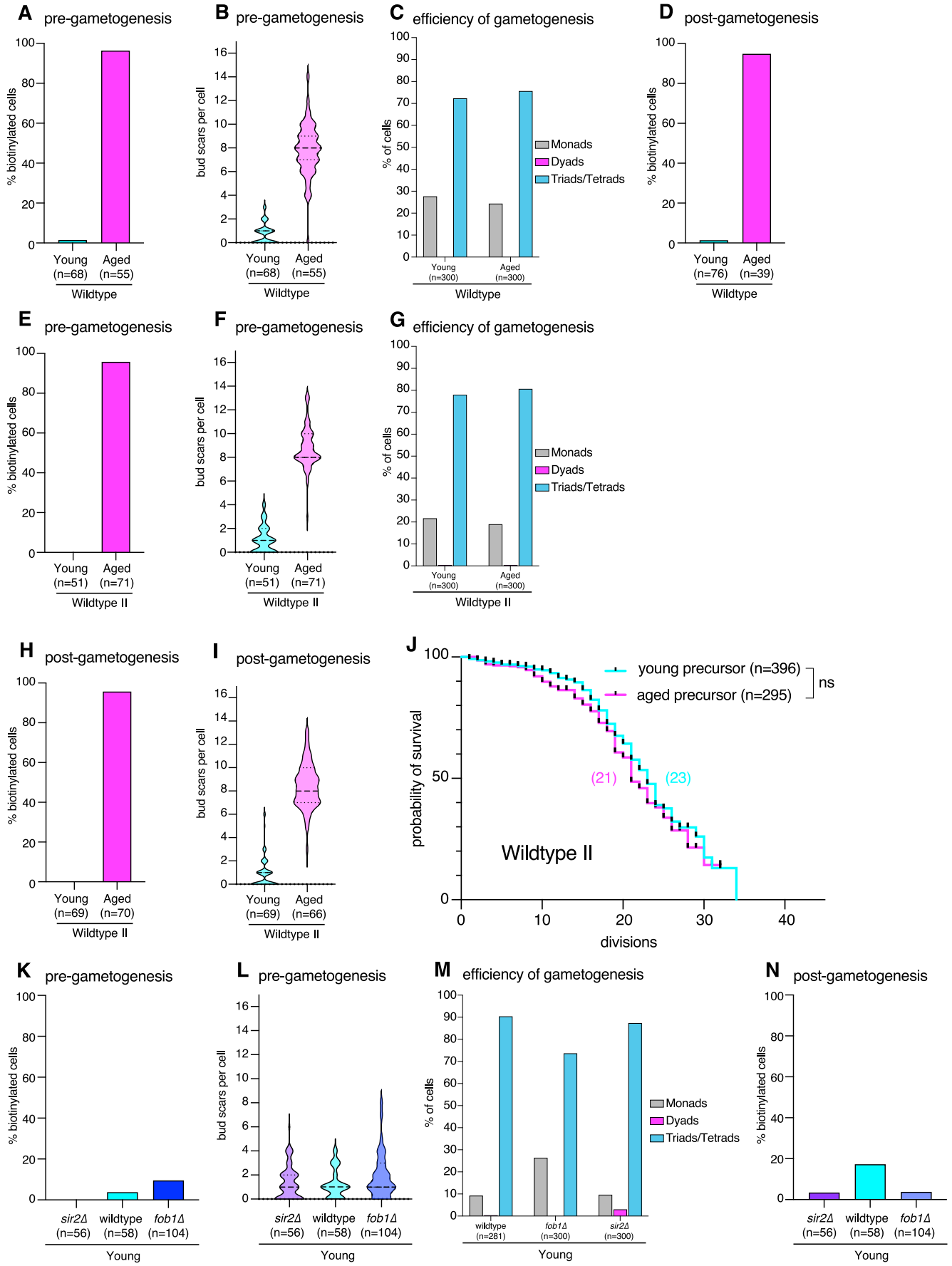
A pre-gametogenesis
% biotinylated cells
Young (n=68)
Aged (n=55)
Wildtype
B pre-gametogenesis
bud scars per cell
Young (n=68)
Aged (n=55)
Wildtype
C efficiency of gametogenesis
% of cells
Monads
Dyads
Triads/Tetrads
Young (n=300)
Aged (n=300)
Wildtype
D post-gametogenesis
% biotinylated cells
Young (n=76)
Aged (n=39)
Wildtype
E pre-gametogenesis
% biotinylated cells
Young (n=51)
Aged (n=71)
Wildtype II
F pre-gametogenesis
bud scars per cell
Young (n=51)
Aged (n=71)
Wildtype II
G efficiency of gametogenesis
% of cells
Monads
Dyads
Triads/Tetrads
Young (n=300)
Aged (n=300)
Wildtype II
H post-gametogenesis
% biotinylated cells
Young (n=69)
Aged (n=70)
Wildtype II
I post-gametogenesis
bud scars per cell
Young (n=69)
Aged (n=66)
Wildtype II
J
young precursor (n=396)
aged precursor (n=295)
ns
(21)
(23)
Wildtype II
probability of survival
divisions
K pre-gametogenesis
% biotinylated cells
sir2Δ (n=56)
wildtype (n=58)
fob1Δ (n=104)
Young
L pre-gametogenesis
bud scars per cell
sir2Δ (n=56)
wildtype (n=58)
fob1Δ (n=104)
Young
M efficiency of gametogenesis
% of cells
Monads
Dyads
Triads/Tetrads
wildtype (n=281)
fob1Δ (n=300)
sir2Δ (n=300)
Young
N post-gametogenesis
% biotinylated cells
sir2Δ (n=56)
wildtype (n=58)
fob1Δ (n=104)
Young

Figure S3. Wildtype gametes completely reset replicative lifespan during gametogenesis.
(**A**) Fraction of biotinylated cells in young (1.5%, 95% CI: 0.3–7.9%, n=68) and aged (96.4%, 95% CI: 87.7–99.0%, n=55) wildtype cell populations.
(**B**) Quantification of replicative age by assessing number of bud scars in young (0.72± 0.84, mean ± SD, n=68) and aged (7.8 ± 2.2, mean ± SD, n=55) wildtype cell populations.
(**C**) Fraction of tetrads in young (72.3%, 95% CI: 67.0–77.1%, n=300) and aged (75.7%, 95% CI: 70.5–80.2% n=300) post gametogenic cell populations.
(**D**) Fraction of biotinylated tetrads in young (1.3%, 95% CI: 0.2–7.1%, n=76) and aged (94.9%, 95% CI: 83.1–98.6%, n=39) wildtype populations after completion of gametogenesis.
(**E**) Fraction of biotinylated cells in young (none, n=51) and aged (95.8%, 95% CI: 88.3–98.6%, n=71) wildtype cell populations.
(**F**) Quantification of replicative age by assessing number of bud scars in young (1.04± 1.1, mean ± SD, n=51) and aged (8.8 ± 1.7, mean ± SD, n=71) wildtype cell populations.
(**G**) Fraction of tetrads in young (78%, 95% CI: 73.0–82.3%, n=300) and aged (80.7%, 95% CI: 75.8–84.7% n=300) post gametogenic cell populations.
(**H**) Fraction of biotinylated tetrads in young (none, n=76) and aged (95.7%, 95% CI: 88.1–98.5%, n=70) wildtype II populations after completion of gametogenesis.
(**I**) Quantification of replicative age by assessing number of bud scars in young (0.9± 1.3, mean ± SD, n=69) and aged (8.4± 1.9, mean ± SD, n=66) wildtype II gamete populations.
(**J**) Quantification of replicative lifespan of young (median lifespan=23, n=396, 274 censored subjects) and aged (median lifespan=21, n=295, 205 censored subjects, p=0.1341 compared to young) wildtype II gametes.
(**K**) Fraction of biotinylated cells in young *sir2*Δ (none, n=78), wildtype (3.7%, 95% CI: 1–12.5%, n=54) and *fob1*Δ (9.5%, 95% CI: 3.8– 22.1%, n=42) cell populations.
(**L**) Quantification of replicative age by assessing number of bud scars in young *sir2*Δ (1.3± 1.4, mean ± SD, n=79), wildtype (1.2 ± 1.2, mean ± SD, n=54) and *fob1*Δ (1.9 ± 1.8, mean ± SD, n=42) cell populations.
(**M**) Fraction of tetrads in young *sir2*Δ (87.3 %, 95% CI: 83.1– 90.6%, n=300), wildtype (90.4 %, 95% CI: 86.4% – 93.3%, n=281) and *fob1*Δ (73.7%, 95% CI: 68.4–78.3%, n=300) post gametogenic cell populations.
(**N**) Fraction of biotinylated tetrads in young *sir2*Δ (3.4%, 95% CI: 1.0–11.7%, n=58), wildtype (17.3%, 95% CI: 11.2–25.7%, n=104) and *fob1*Δ (3.8%, 95% CI: 1.0–12.8%, n=53) populations after completion of gametogenesis.
Confidence intervals were calculated using the Wilson score method and statistical significance for differences between replicative lifespans was calculated using the Log-rank (Mantel-cox) test, tick marks on survival curves represent censored events.

Figure S4

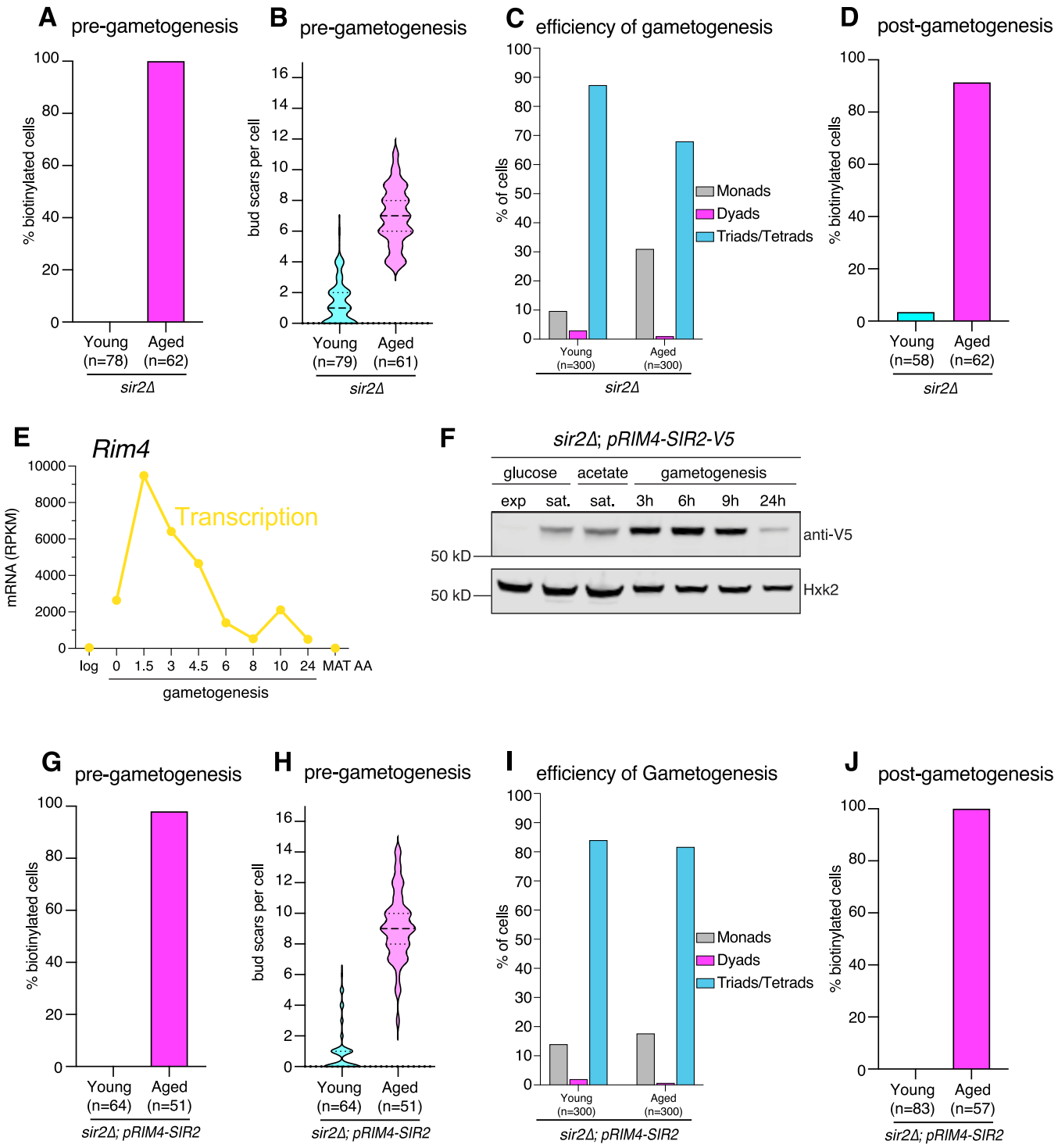
A
pre-gametogenesis
% biotinylated cells
Young (n=78)
Aged (n=62)
sir2Δ
B
pre-gametogenesis
bud scars per cell
Young (n=79)
Aged (n=61)
sir2Δ
C
efficiency of gametogenesis
% of cells
Monads
Dyads
Triads/Tetrads
Young (n=300)
Aged (n=300)
sir2Δ
D
post-gametogenesis
% biotinylated cells
Young (n=58)
Aged (n=62)
sir2Δ
E
Rim4
Transcription
mRNA (RPKM)
log
0
1.5
3
4.5
6
8
10
24
MAT AA
gametogenesis
F
sir2Δ; pRIM4-SIR2-V5
glucose
acetate
gametogenesis
exp
sat.
sat.
3h
6h
9h
24h
anti-V5
50 kD
Hxk2
50 kD
G
pre-gametogenesis
% biotinylated cells
Young (n=64)
Aged (n=51)
sir2Δ; pRIM4-SIR2
H
pre-gametogenesis
bud scars per cell
Young (n=64)
Aged (n=51)
sir2Δ; pRIM4-SIR2
I
efficiency of Gametogenesis
% of cells
Monads
Dyads
Triads/Tetrads
Young (n=300)
Aged (n=300)
sir2Δ; pRIM4-SIR2
J
post-gametogenesis
% biotinylated cells
Young (n=83)
Aged (n=57)
sir2Δ; pRIM4-SIR2

Figure S4. *sir2*Δ mutants and gametogenesis specific Sir2 expression both fail to reset replicative lifespan of gametes

(**A**) Fraction of biotinylated cells in young (none, n=78, same data as shown in Fig. 4A) and aged (all, n=78) *sir2*Δ cell populations.

(**B**) Quantification of replicative age by assessing number of bud scars in young (1.3± 1.4, mean ± SD, n=79, same data as shown in Fig. 4B) and aged (7± 1.9, mean ± SD, n=61) *sir2*Δ cell populations.

(**C**) Fraction of tetrads in young (87.3% 95% CI: 83.1–90.6% n=300, same data as shown in Fig. 4E) and aged (68.0% (95% CI: 62.5–73.0%, n=300) post gametogenic *sir2*Δ cell populations.

(**D**) Fraction of biotinylated tetrads in young (3.4%, 95% CI: 1.0–11.7%, n=58, same data as shown in Fig. 4C) and aged (91.9%, 95% CI: 82.5–96.5%, n=62) *sir2*Δ populations after completion of gametogenesis.

(**E**) *RIM4* transcript levels (RNA-seq) either during log-phase vegetative growth in 2% glucose containing media (log), the indicated time in gametogenesis inducing media (h), or in control diploids that cannot undergo gametogenesis (*MAT*a/a) plotted from previously generated meiotic datasets (Cheng et al., 2018).

(**F**) Immunoblot to quantify Sir2-V5 levels driven by *RIM4* promoter fragment (anti-V5) and loading control (Hxk2) in growth media containing ether 2% glucose (glucose) or acetate (acetate) and at different timepoints upon transfer to gametogenesis-inducing media (gametogenesis).

(**G**) Fraction of biotinylated cells in young (none, n=64) and aged (98.0%, 95% CI: 89.7–99.7%, n=51) *pRIM4-SIR2 sir2*Δ cell populations.

(**H**) Quantification of replicative age by assessing number of bud scars in young (0.98± 1.5, mean ± SD, n=64) and aged (9.1± 2.2 (mean ± SD, n=51) *pRIM4-SIR2 sir2*Δ cell populations.

(**I**) Fraction of tetrads in young (84 %, 95% CI: 79.4–87.7%, n=300) and aged (81.7%, 95% CI: 76.9–85.6%, n=300) post gametogenic *pRIM4-SIR2 sir2*Δ cell populations.

(**J**) Fraction of biotinylated tetrads in young (none, n=83) and aged (all, n=57) *pRIM4-SIR2 sir2*Δ populations after completion of gametogenesis. Confidence intervals were calculated using the Wilson score method.

Figure S5

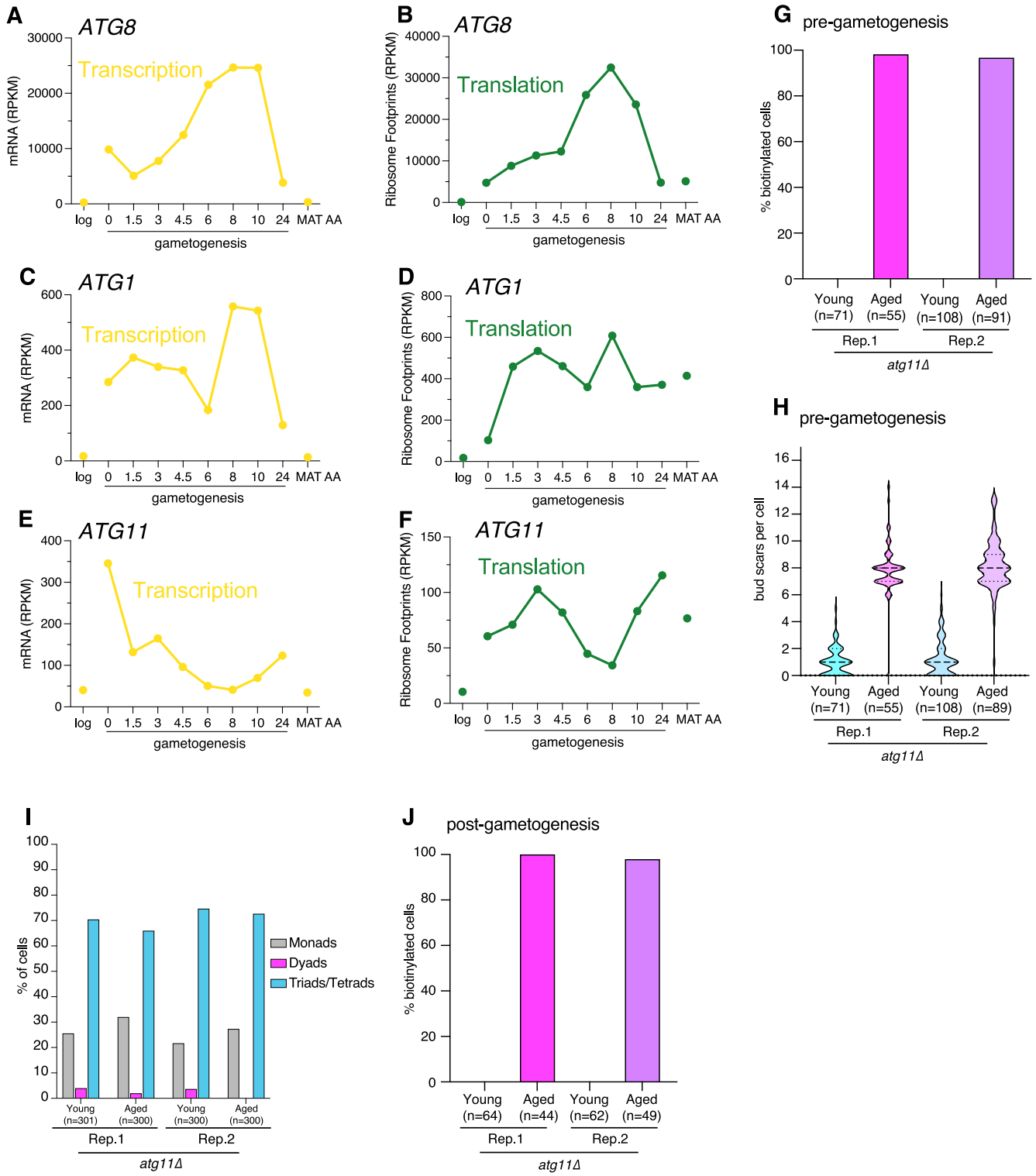
A
ATG8
Transcription
mRNA (RPKM)
30000
20000
10000
0
log 0 1.5 3 4.5 6 8 10 24 MAT AA
gametogenesis
B
ATG8
Translation
Ribosome Footprints (RPKM)
40000
30000
20000
10000
0
log 0 1.5 3 4.5 6 8 10 24 MAT AA
gametogenesis
G
pre-gametogenesis
% biotinylated cells
100
80
60
40
20
0
Young (n=71)
Aged (n=55)
Young (n=108)
Aged (n=91)
Rep.1
Rep.2
atg11Δ
C
ATG1
Transcription
mRNA (RPKM)
600
400
200
0
log 0 1.5 3 4.5 6 8 10 24 MAT AA
gametogenesis
D
ATG1
Translation
Ribosome Footprints (RPKM)
800
600
400
200
0
log 0 1.5 3 4.5 6 8 10 24 MAT AA
gametogenesis
H
pre-gametogenesis
bud scars per cell
16
14
12
10
8
6
4
2
0
Young (n=71)
Aged (n=55)
Young (n=108)
Aged (n=89)
Rep.1
Rep.2
atg11Δ
E
ATG11
Transcription
mRNA (RPKM)
400
300
200
100
0
log 0 1.5 3 4.5 6 8 10 24 MAT AA
gametogenesis
F
ATG11
Translation
Ribosome Footprints (RPKM)
150
100
50
0
log 0 1.5 3 4.5 6 8 10 24 MAT AA
gametogenesis
I
% of cells
100
90
80
70
60
50
40
30
20
10
0
Monads
Dyads
Triads/Tetrads
Young (n=301)
Aged (n=300)
Young (n=300)
Aged (n=300)
Rep.1
Rep.2
atg11Δ
J
post-gametogenesis
% biotinylated cells
100
80
60
40
20
0
Young (n=64)
Aged (n=44)
Young (n=62)
Aged (n=49)
Rep.1
Rep.2
atg11Δ

Figure S5. *atg11*Δ mutants fail to reset replicative lifespan of gametes

(**A-F**) Expression of autophagy factors either during log-phase vegetative growth in 2% glucose containing media (log), the indicated time in gametogenesis inducing media (h), or in control diploids that cannot undergo gametogenesis (*MAT*a/a) plotted from previously generated meiotic datasets (Cheng et al., 2018).

(**A**) *ATG8* transcript levels (RNA-seq).

(**B**) *ATG8* translation levels (ribosome-protected footprints).

(**C**) *ATG1* transcript levels (RNA-seq).

(**D**) *ATG1* translation levels (ribosome-protected footprints).

(**E**) *ATG11* transcript levels (RNA-seq).

(**F**) *ATG11* translation levels (ribosome-protected footprints).

(**G**) Fraction of biotinylated cells in *atg11*Δ cell populations: Replicate 1 (Rep. 1) young (none, n=71) and aged (98.2%, 95% CI: 90.4–99.7%, n=55); Replicate 2 (Rep. 2) young (none, n=108) and aged (96.7%, 95% CI: 90.8–98.9%, n=91).

(**H**) Quantification of replicative age by assessing number of bud scars in *atg11*Δ cell populations: Rep. 1 young (1 ± 1.1, mean ± SD, n=71) and aged (7.9± 1.9, mean ± SD, n=55); Rep. 2 young (1.2 ± 1.3, mean ± SD, n=108) and aged (8.2± 1.9, mean ± SD, n=89).

(**I**) Fraction of tetrads in post gametogenic *atg11*Δ cell populations: Rep.1 young (70.4%, 95% CI: 65.0–75.3%), n=301) and aged (66.0%, 95% CI: 60.5–71.1%, n=300); Rep. 2 young (74.7%, 95% CI: 69.5–79.3%, n=300) and aged (72.7%, 95% CI: 67.4–77.4%, n=300).

(**J**) Fraction of biotinylated tetrads in *atg11*Δ populations after completion of gametogenesis: Rep.1 young (none, n=64) and aged (all, n=44; Rep. 2 young (none, n=62) and aged (98%, 95% CI: 89.3–99.6%, n=91all, n=49). Confidence intervals were calculated using the Wilson score method.

Figure S6

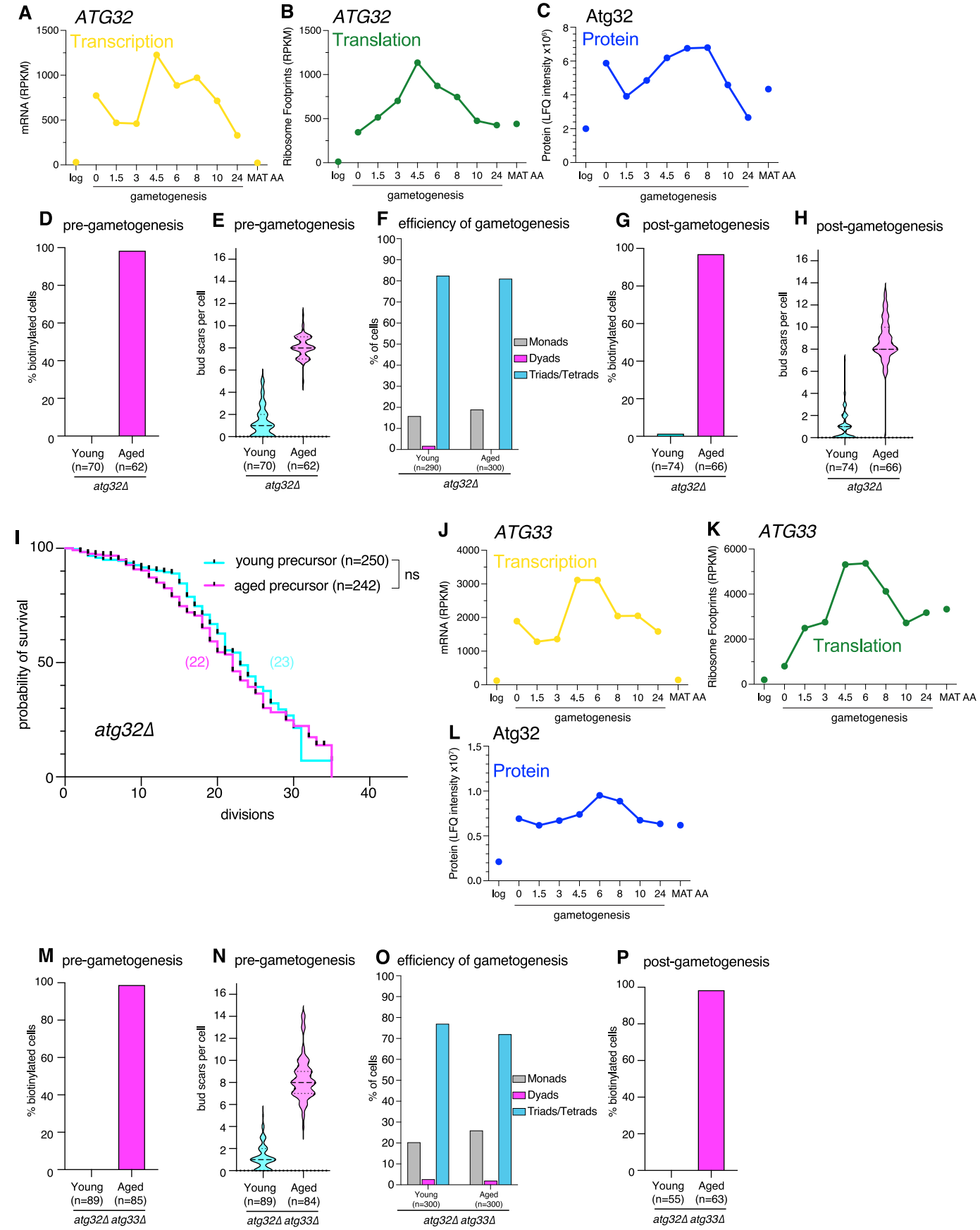
A
ATG32
Transcription
mRNA (RPKM)
gametogenesis
B
ATG32
Translation
Ribosome Footprints (RPKM)
gametogenesis
C
Atg32
Protein
Protein (LFQ intensity x10⁶)
gametogenesis
log 0 1.5 3 4.5 6 8 10 24 MAT AA
D pre-gametogenesis
% biotinylated cells
Young (n=70) Aged (n=62)
atg32Δ
E pre-gametogenesis
bud scars per cell
Young (n=70) Aged (n=62)
atg32Δ
F efficiency of gametogenesis
% of cells
Monads
Dyads
Triads/Tetrads
Young (n=290) Aged (n=300)
atg32Δ
G post-gametogenesis
% biotinylated cells
Young (n=74) Aged (n=66)
atg32Δ
H post-gametogenesis
bud scars per cell
Young (n=74) Aged (n=66)
atg32Δ
I
probability of survival
young precursor (n=250)
aged precursor (n=242)
ns
(22)
(23)
atg32Δ
divisions
J
ATG33
Transcription
mRNA (RPKM)
gametogenesis
K
ATG33
Translation
Ribosome Footprints (RPKM)
gametogenesis
L
Atg32
Protein
Protein (LFQ intensity x10⁷)
gametogenesis
M pre-gametogenesis
% biotinylated cells
Young (n=89) Aged (n=85)
atg32Δ atg33Δ
N pre-gametogenesis
bud scars per cell
Young (n=89) Aged (n=84)
atg32Δ atg33Δ
O efficiency of gametogenesis
% of cells
Monads
Dyads
Triads/Tetrads
Young (n=300) Aged (n=300)
atg32Δ atg33Δ
P post-gametogenesis
% biotinylated cells
Young (n=55) Aged (n=63)
atg32Δ atg33Δ

Figure S6. *atg32*Δ mutants and *atg32*Δ *atg33*Δ double mutants completely reset replicative lifespan of gametes

(**A-C & J-L**) Expression levels either during log-phase vegetative growth in 2% glucose containing media (log), the indicated time in gametogenesis inducing media (h), or in control diploids that cannot undergo gametogenesis (*MAT*a/a) plotted from previously generated meiotic datasets (Cheng et al., 2018).

(**A**) *ATG32* transcript levels (RNA-seq).

(**B**) *ATG32* translation levels (ribosome-protected footprints).

(**C**) Atg32 protein levels (mass spectrometry).

(**D**) Fraction of biotinylated cells in young (none, n=70) and aged (98.4%, 95% CI: 91.4–99.7%, n=62) *atg32*Δ cell populations.

(**E**) Quantification of replicative age by assessing number of bud scars in young (1.3± 1.4, mean ± SD, n=70) and aged (8.1± 0.98, mean ± SD, n=62) *atg32*Δ cell populations.

(**F**) Fraction of tetrads in young (82.4%, 95% CI: 77.6–86.4%), n=290) and aged (81.0%, 95% CI: 76.2–85.0%, n=300) post-gametogenic *atg32*Δ cell populations.

(**G**) Fraction of biotinylated tetrads in young (1.4%, 95% CI: 0.2–7.3%, n=74) and aged 97.0% (95% CI: 89.6–99.2%, n=66) *atg32*Δ populations after completion of gametogenesis.

(**H**) Quantification of replicative age by assessing number of bud scars in young (0.93± 1.3, mean ± SD, n=74) and aged (8.7± 2, mean ± SD, n=66) *atg32*Δ gamete populations.

(**I**) Quantification of replicative lifespan of young (median lifespan=23, n=242, 151 censored subjects, 1 technical replicate) and aged (median lifespan=22, n=250, 151 censored subjects, p=0.2691) *atg32*Δ gametes.

(**J**) *ATG33* transcript levels (RNA-seq).

(**K**) *ATG33* translation levels (ribosome-protected footprints).

(**L**) Atg33 protein levels (mass spectrometry).

(**M**) Fraction of biotinylated cells in young (none, n=89) and aged (98.8%, 95% CI: 93.6–99.8%, n=85) *atg32*Δ *atg33*Δ double mutant cell populations.

(**N**) Quantification of replicative age by assessing number of bud scars in young (1.2± 1.1, mean ± SD, n=89) and aged (8.4± 2, mean ± SD, n=84) *atg32*Δ *atg33*Δ double mutants.

(**O**) Fraction of tetrads in young (77.0%, 95% CI: 71.9–81.4%, n=300) and aged (72.0%, 95% CI: 66.7–76.8%, n=300) post gametogenic *atg32*Δ *atg33*Δ cell populations.

(**P**) Fraction of biotinylated tetrads in young (none, n=55) and aged (98.4%, 95% CI: 91.5–99.7%, n=63) *atg32*Δ *atg33*Δ populations after completion of gametogenesis.

Confidence intervals were calculated using the Wilson score method and statistical significance for differences between replicative lifespans was calculated using the Log-rank (Mantel-cox) test, tick marks on survival curves represent censored events.

Figure S7

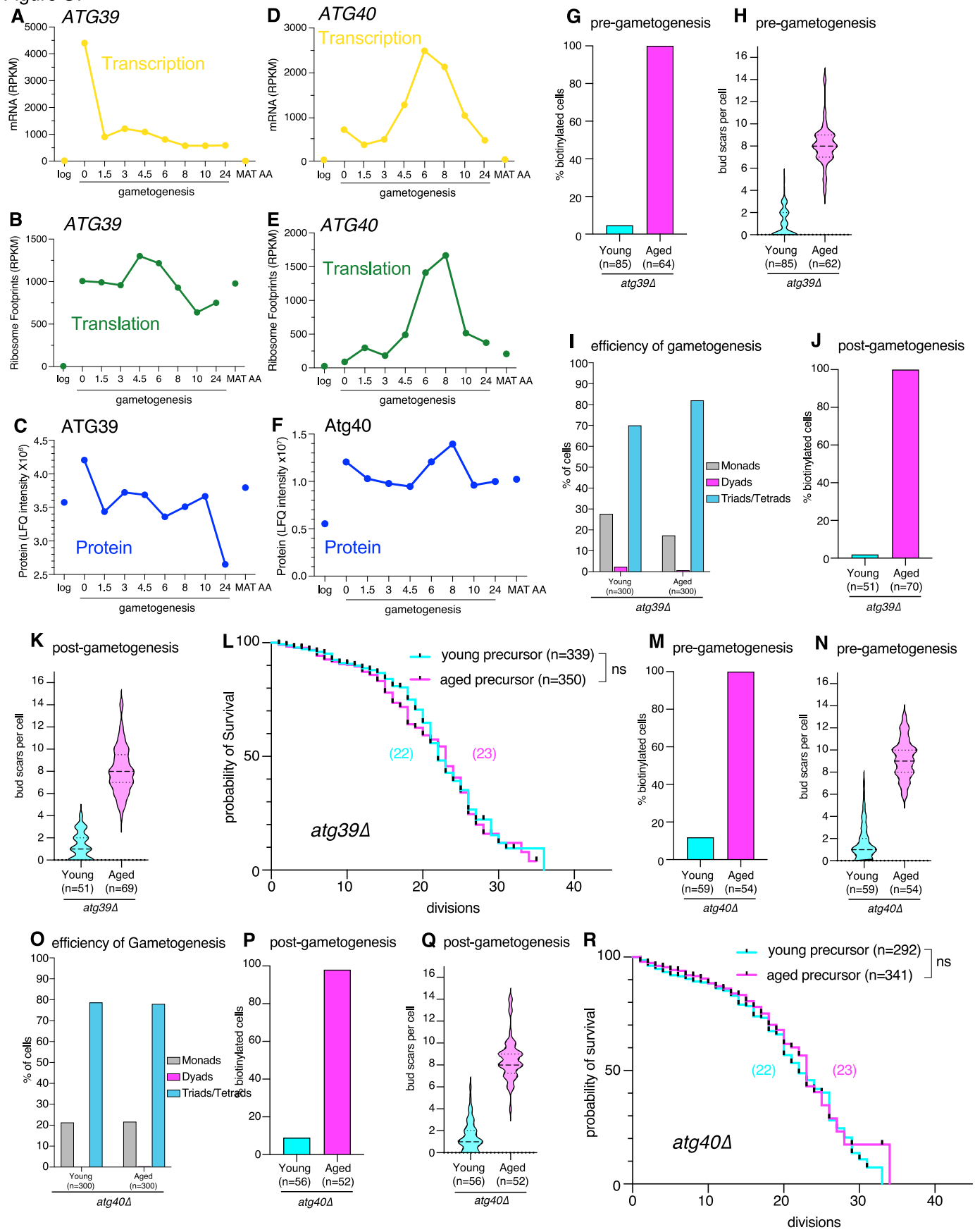
A ATG39
mRNA (RPKM)
Transcription
log 0 1.5 3 4.5 6 8 10 24 MAT AA
gametogenesis
B ATG39
Ribosome Footprints (RPKM)
Translation
C ATG39
Protein (LFQ intensity X10⁶)
Protein
D ATG40
Transcription
E ATG40
Translation
F Atg40
Protein (LFQ intensity x10⁷)
Protein
G pre-gametogenesis
% biotinylated cells
Young (n=85)
Aged (n=64)
atg39Δ
H pre-gametogenesis
bud scars per cell
Young (n=85)
Aged (n=62)
atg39Δ
I efficiency of gametogenesis
% of cells
Monads
Dyads
Triads/Tetrads
Young (n=300)
Aged (n=300)
atg39Δ
J post-gametogenesis
% biotinylated cells
Young (n=51)
Aged (n=70)
atg39Δ
K post-gametogenesis
bud scars per cell
Young (n=51)
Aged (n=69)
atg39Δ
L
probability of Survival
young precursor (n=339)
aged precursor (n=350)
ns
(22)
(23)
atg39Δ
divisions
M pre-gametogenesis
% biotinylated cells
Young (n=59)
Aged (n=54)
atg40Δ
N pre-gametogenesis
bud scars per cell
Young (n=59)
Aged (n=54)
atg40Δ
O efficiency of Gametogenesis
% of cells
Monads
Dyads
Triads/Tetrads
Young (n=300)
Aged (n=300)
atg40Δ
P post-gametogenesis
biotinylated cells
Young (n=56)
Aged (n=52)
atg40Δ
Q post-gametogenesis
bud scars per cell
Young (n=56)
Aged (n=52)
atg40Δ
R
probability of survival
young precursor (n=292)
aged precursor (n=341)
ns
(22)
(23)
atg40Δ
divisions

Figure S7. *atg39*Δ and *atg40*Δ single mutants reset replicative lifespan during gametogenesis

(**A-F**) Expression of *ATG39* and *ATG40* either during log-phase vegetative growth in 2% glucose containing media (log), the indicated time in gametogenesis inducing media (h), or in control diploids that cannot undergo gametogenesis (*MAT*a/a) plotted from previously generated meiotic datasets (Cheng et al., 2018).

(**A**) *ATG39* transcript levels (RNA-seq).

(**B**) *ATG39* translation levels (ribosome-protected footprints).

(**C**) Atg39 protein levels (mass spectrometry).

(**D**) *ATG40* transcript levels (RNA-seq).

(**E**) *ATG40* translation levels (ribosome-protected footprints).

(**F**) Atg40 protein levels (mass spectrometry).

(**G**) Fraction of biotinylated cells in young (3.5%, 95% CI: 1.2–9.9%, n=85) and aged (all, n=64) *atg39*Δ cell populations.

(**H**) Quantification of replicative age by assessing number of bud scars in young (0.98± 1.2, mean ± SD, n=85) and aged (8.1± 1.8, mean ± SD, n=64) *atg39*Δ cell populations.

(**I**) Fraction of tetrads in young (70.0%, 95% CI: 64.6–74.9%, n=300) and aged (82.0% (95% CI: 77.3–85.9%, n=300) post gametogenic *atg39*Δ cell populations.

(**J**) Fraction of biotinylated tetrads in young (2.0%, 95% CI: 0.3–10.3%, n=51) and aged (all, n=69) *atg39*Δ populations after completion of gametogenesis.

(**K**) Quantification of replicative age by assessing number of bud scars in young (1.3± 1.2, mean ± SD, n=51) and aged (8.1± 2.1, mean ± SD, n=69) *atg39*Δ gamete populations.

(**L**) Quantification of replicative lifespan of young (median lifespan=22, n=339, 188 censored subjects) and aged *atg39*Δ (median lifespan=23, n=350, 225 censored subjects, p=0.418 compared to young) gametes.

(**M**) Fraction of biotinylated cells in young (11.9%, 95% CI: 5.9–22.5%, n=59) and aged (all, n=54) *atg40*Δ cell populations.

(**N**) Quantification of replicative age by assessing number of bud scars in young (1.6± 1.6, mean ± SD, n=59) and aged (9.3± 1.8, mean ± SD, n=54) *atg40*Δ cell populations.

(**O**) Fraction of tetrads in young (78.7%, 95% CI: 73.7–82.9%, n=300) and aged (78.0%, 95% CI: 73.0–82.3%, n=300) post gametogenic *atg39*Δ cell populations.

(**P**) Fraction of biotinylated tetrads in young (8.9%, 95% CI: 3.9–19.3%, n=56) and aged (98.1%, 95% CI: 89.9–99.7%, n=52) *atg40*Δ populations after completion of gametogenesis.

(**Q**) Quantification of replicative age by assessing number of bud scars in young (1.4± 1.4, mean ± SD, n=56), and aged (8.6± 1.9, mean ± SD, n=52) *atg40*Δ gamete populations.

(**R**) Quantification of replicative lifespan of young (median lifespan=22, n=292, 176 censored subjects) and aged *atg40*Δ (median lifespan=23, n=341, 256 censored subjects, p=0.389 compared to young) gametes.

Confidence intervals were calculated using the Wilson score method and statistical significance for differences between replicative lifespans was calculated using the Log-rank (Mantel-cox) test, tick marks on survival curves represent censored events.

Figure S8

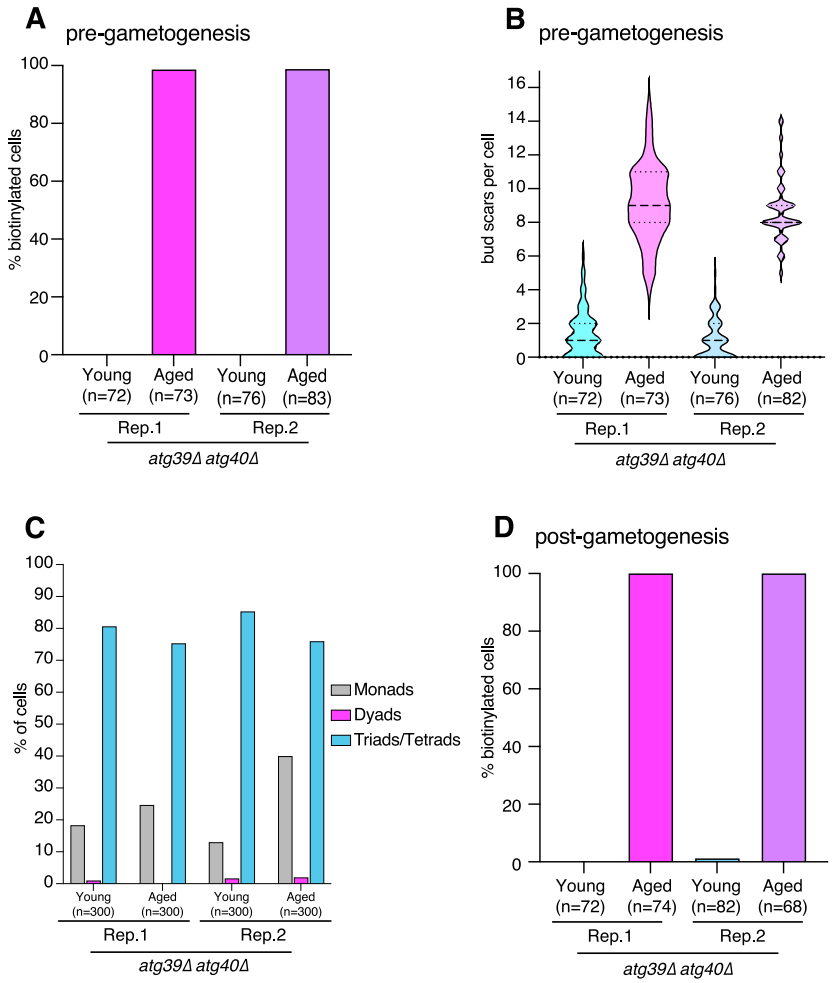

Figure S8. *atg39*Δ *atg40*Δ double mutants fail to reset replicative lifespan during gametogenesis

(**A**) Fraction of biotinylated cells in *atg39*Δ *atg40*Δ cell populations: Replicate 1 (Rep. 1) young (none, n=72) and aged (98.6%, 95% CI: 92.6–99.8%, n=73); Replicate 2 (Rep. 2) young (none, n=76) and aged (98.8%, 95% CI: 93.5–99.8%, n=83).

(**B**) Quantification of replicative age by assessing number of bud scars in *atg39*Δ *atg40*Δ cell populations: Rep. 1 young (1.4± 1.4, mean ± SD, n=72) and aged (9.1± 2.3, mean ± SD, n=73); Rep. 2 young (1 ± 1.2, mean ± SD, n=76) and aged (8.7± 1.9, mean ± SD, n=82).

(**C**) Fraction of tetrads in post gametogenic *atg39*Δ *atg40*Δ cell populations: Rep.1 young (80.7%, 95% CI: 75.8–84.7%, n=300) and aged (75.3%, 95% CI: 70.2–79.9%, n=300); Rep. 2 young (85.3%, 95% CI: 80.9–88.9%, n=300) and aged (76.0%, 95% CI: 70.9–80.5%, n=300).

(**D**) Fraction of biotinylated tetrads in *atg39*Δ *atg40*Δ populations after completion of gametogenesis: Rep.1 young (none, n=72) and aged (all, n=74); Rep. 2 young (1.2%, 95% CI: 0.2–6.6%, n=82) and aged (all, n=68).

Confidence intervals were calculated using the Wilson score method.

Figure S9

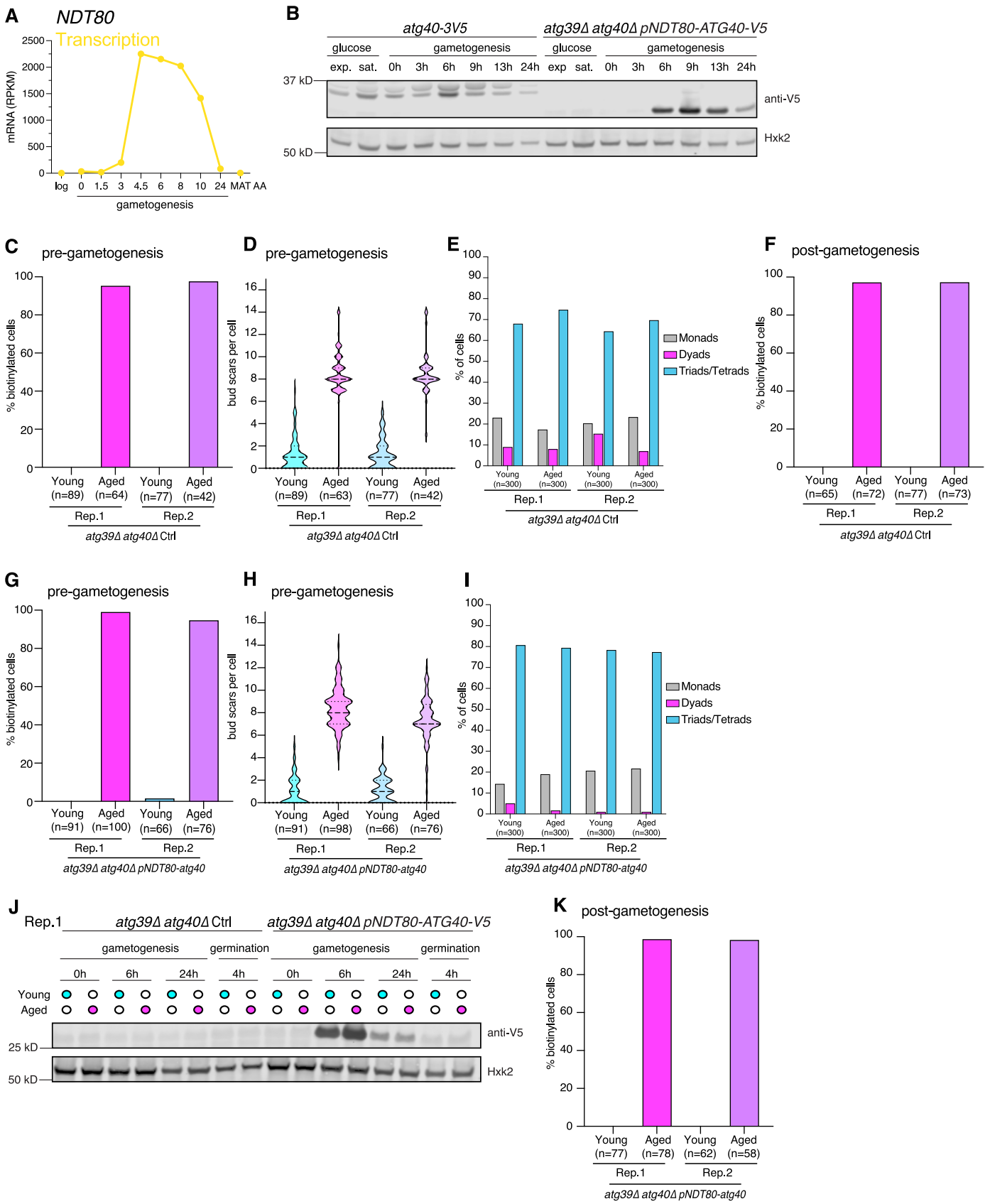
A
NDT80
Transcription
mRNA (RPKM)
2500
2000
1500
1000
500
0
log 0 1.5 3 4.5 6 8 10 24 MAT AA
gametogenesis
B
atg40-3V5
atg39Δ atg40Δ pNDT80-ATG40-V5
glucose
gametogenesis
exp. sat. 0h 3h 6h 9h 13h 24h exp sat. 0h 3h 6h 9h 13h 24h
37 kD
50 kD
anti-V5
Hxk2
C
pre-gametogenesis
% biotinylated cells
Young (n=89) Aged (n=64) Young (n=77) Aged (n=42)
Rep.1 Rep.2
atg39Δ atg40Δ Ctrl
D
pre-gametogenesis
bud scars per cell
Young (n=89) Aged (n=63) Young (n=77) Aged (n=42)
Rep.1 Rep.2
atg39Δ atg40Δ Ctrl
E
% of cells
Monads
Dyads
Triads/Tetrads
Young (n=300) Aged (n=300) Young (n=300) Aged (n=300)
Rep.1 Rep.2
atg39Δ atg40Δ Ctrl
F
post-gametogenesis
% biotinylated cells
Young (n=65) Aged (n=72) Young (n=77) Aged (n=73)
Rep.1 Rep.2
atg39Δ atg40Δ Ctrl
G
pre-gametogenesis
% biotinylated cells
Young (n=91) Aged (n=100) Young (n=66) Aged (n=76)
Rep.1 Rep.2
atg39Δ atg40Δ pNDT80-atg40
H
pre-gametogenesis
bud scars per cell
Young (n=91) Aged (n=98) Young (n=66) Aged (n=76)
Rep.1 Rep.2
atg39Δ atg40Δ pNDT80-atg40
I
% of cells
Monads
Dyads
Triads/Tetrads
Young (n=300) Aged (n=300) Young (n=300) Aged (n=300)
Rep.1 Rep.2
atg39Δ atg40Δ pNDT80-atg40
J
Rep.1
atg39Δ atg40Δ Ctrl
atg39Δ atg40Δ pNDT80-ATG40-V5
gametogenesis
germination
0h 6h 24h 4h 0h 6h 24h 4h
Young
Aged
25 kD
50 kD
anti-V5
Hxk2
K
post-gametogenesis
% biotinylated cells
Young (n=77) Aged (n=78) Young (n=62) Aged (n=58)
Rep.1 Rep.2
atg39Δ atg40Δ pNDT80-atg40

Figure S9. Supporting data for meiosis specific expression of *ATG40* is sufficient to rescue reset of replicative lifespan in cells that lack *ATG40 and ATG39*

A) *NDT80* transcript levels (RNA-seq) either during log-phase vegetative growth in 2% glucose containing media (log), the indicated time in gametogenesis inducing media (h), or in control diploids that cannot undergo gametogenesis (*MAT*a/a) plotted from previously generated meiotic datasets (Cheng et al., 2018).

(**B**) Immunoblot comparing endogenous Atg40-3V5 to pNDT80-Atg40-V5 rescue construct protein levels (anti-V5) and loading control (Hxk2) during exponential and saturated growth in media containing 2% glucose (glucose) and at different timepoints upon transfer to gametogenesis-inducing media (gametogenesis).

(**C**) Fraction of biotinylated cells in *atg39*Δ *atg40*Δ control cell populations: Replicate 1 (Rep. 1) young (none, n=89) and aged (95.3%, 95% CI: 87.1–98.4%, n=64); Replicate 2 (Rep. 2) young (none, n=77) and aged (97.6%, 95% CI: 87.7–99.6%, n=44).

(**D**) Quantification of replicative age by assessing number of bud scars in *atg39*Δ *atg40*Δ control cell populations: Rep. 1 young (1.2± 1.4, mean ± SD, n=89) and aged (8.5± 1.9, mean ± SD, n=63); Rep. 2 young (1.3 ± 1.3, mean ± SD, n=77) and aged (8.5± 1.9, mean ± SD, n=42).

(**E**) Fraction of tetrads in post gametogenic *atg39*Δ *atg40*Δ control cell populations: Rep.1 young (68.0%, 95% CI: 62.5–73.0%, n=300) and aged (74.7%, 95% CI: 69.5–79.3%, n=300); Rep. 2 young (64.3%, 95% CI: 58.8–69.5%, n=300) and aged (69.7%, 95% CI: 64.2–74.6%, n=300).

(**F**) Fraction of biotinylated tetrads in *atg39*Δ *atg40*Δ control populations after completion of gametogenesis: Rep.1 young (none, n=65) and aged (97.2%, 95% CI: 90.4–99.2%, n=72); Rep. 2 young (none, n=77) and aged (97.3%, 95% CI: 90.5–99.2%, n=73).

(**G**) Fraction of biotinylated cells in *atg39*Δ *atg40*Δ *pNDT80-ATG40* cell populations: Replicate 1 (Rep. 1) young (none, n=91) and aged (99.0%, 95% CI: 94.6–99.8%, n=100); Replicate 2 (Rep. 2) young (1.5%, 95% CI: 0.3–8.1%, n=66) and aged (94.7%, 95% CI: 87.2–97.9%, n=76).

(**H**) Quantification of replicative age by assessing number of bud scars in *atg39*Δ *atg40*Δ *pNDT80-ATG40* cell populations: Rep. 1 young (1.0± 1.3, mean ± SD, n=91) and aged (8.4± 1.3, mean ± SD, n=98); Rep. 2 young (1.1 ± 1.1, mean ± SD, n=66) and aged (7.3± 2.1, mean ± SD, n=76).

(**I**) Fraction of tetrads in post gametogenic *atg39*Δ *atg40*Δ *pNDT80-ATG40* cell populations: Rep.1 young (80.7%, 95% CI: 75.8–84.7%, n=300) and aged (79.3%, 95% CI: 74.4–83.5%, n=300); Rep. 2 young (78.3%, 95% CI: 73.3–82.6%, n=300) and aged (77.3%, 95% CI: 72.3–81.7%, n=300).

(**J**) Immunoblot of young and aged control and pNDT80-Atg40-V5 samples to quantify protein levels (anti-V5) and loading control (Hxk2) at different timepoints upon transfer to gametogenesis-inducing media (gametogenesis) and after re-growth in media containing 2% glucose (germination) (samples collected from Rep.1).

(**K**) Fraction of biotinylated tetrads in *atg39*Δ *atg40*Δ *pNDT80-ATG40* cell populations after completion of gametogenesis: Rep.1 young (none, n=77) and aged (98.7%, 95% CI: 93.1–99.8%, n=78); Rep. 2 young (none, n=62) and aged (98.3%, 95% CI: 90.9–99.7%, n=58). Confidence intervals were calculated using the Wilson score method.

References

Azizoglu, A., Brent, R., Rudolf, F., 2021. A precisely adjustable, variation-suppressed eukaryotic transcriptional controller to enable genetic discovery. eLife 10, e69549. https://doi.org/10.7554/eLife.69549

Bellí, G., Garí, E., Piedrafita, L., Aldea, M., Herrero, E., 1998. An activator/repressor dual system allows tight tetracycline-regulated gene expression in budding yeast. Nucleic Acids Res 26, 942–947. https://doi.org/10.1093/nar/26.4.942

Boselli, M., Rock, J., Ünal, E., Levine, S.S., Amon, A., 2009. Effects of Age on Meiosis in Budding Yeast. Developmental Cell 16, 844–855. https://doi.org/10.1016/j.devcel.2009.05.013

Cabib, E., Bowers, B., 1971. Chitin and Yeast Budding: LOCALIZATION OF CHITIN IN YEAST BUD SCARS. Journal of Biological Chemistry 246, 152–159. https://doi.org/10.1016/S0021-9258(18)62543-8

Carmelo, V., Santos, H., Sá-Correia, I., 1997. Effect of extracellular acidification on the activity of plasma membrane ATPase and on the cytosolic and vacuolar pH of Saccharomyces cerevisiae. Biochim Biophys Acta 1325, 63–70. https://doi.org/10.1016/s0005-2736(96)00245-3

Chen, K.L., Crane, M.M., Kaeberlein, M., 2017. Microfluidic Technologies for Yeast Replicative Lifespan Studies. Mech Ageing Dev 161, 262–269. https://doi.org/10.1016/j.mad.2016.03.009

Cheng, Z., Mugler, C.F., Keskin, A., Hodapp, S., Chan, L.Y.-L., Weis, K., Mertins, P., Regev, A., Jovanovic, M., Brar, G.A., 2019. Small and Large Ribosomal Subunit Deficiencies Lead to Distinct Gene Expression Signatures that Reflect Cellular Growth Rate. Molecular Cell 73, 36-47.e10. https://doi.org/10.1016/j.molcel.2018.10.032

Cheng, Z., Otto, G.M., Powers, E.N., Keskin, A., Mertins, P., Carr, S.A., Jovanovic, M., Brar, G.A., 2018. Pervasive, Coordinated Protein-Level Changes Driven by Transcript Isoform Switching during Meiosis. Cell 172, 910-923.e16. https://doi.org/10.1016/j.cell.2018.01.035

Chol, K.-Y., Satterberg, B., Lyons, D.M., Elion, E.A., 1994. Ste5 tethers multiple protein kinases in the MAP kinase cascade required for mating in S. cerevisiae. Cell 78, 499–512. https://doi.org/10.1016/0092-8674(94)90427-8

Defossez, P.-A., Prusty, R., Kaeberlein, M., Lin, S.-J., Ferrigno, P., Silver, P.A., Keil, R.L., Guarente, L., 1999. Elimination of Replication Block Protein Fob1 Extends the Life Span of Yeast Mother Cells. Molecular Cell 3, 447–455. https://doi.org/10.1016/S1097-2765(00)80472-4

Deng, C., Saunders, W., 2001. RIM4 encodes a meiotic activator required for early events of meiosis in Saccharomyces cerevisiae. Mol Gen Genomics 266, 497–504. https://doi.org/10.1007/s004380100571

Denoth Lippuner, A., Julou, T., Barral, Y., 2014. Budding yeast as a model organism to study the effects of age. FEMS Microbiol Rev 38, 300–325. https://doi.org/10.1111/1574-6976.12060

Dikic, I., Elazar, Z., 2018. Mechanism and medical implications of mammalian autophagy. Nat Rev Mol Cell Biol 19, 349–364. https://doi.org/10.1038/s41580-018-0003-4

Fang, O., Hu, X., Wang, L., Jiang, N., Yang, J., Li, B., Luo, Z., 2018. Amn1 governs post-mitotic cell separation in Saccharomyces cerevisiae. PLOS Genetics 14, e1007691. https://doi.org/10.1371/journal.pgen.1007691

Farré, J.-C., Subramani, S., 2016. Mechanistic insights into selective autophagy pathways: lessons from yeast. Nat Rev Mol Cell Biol 17, 537–552. https://doi.org/10.1038/nrm.2016.74

Fernandes, A.R., Sá-Correia, I., 2003. Transcription patterns of PMA1 and PMA2 genes and activity of plasma membrane H+-ATPase in Saccharomyces cerevisiae during diauxic growth and stationary phase. Yeast 20, 207–219. https://doi.org/10.1002/yea.957

Gao, Z., Xu, J., Chen, K., Wang, S., Ouyang, Q., Luo, C., 2020. Comparative Analysis of Yeast Replicative Lifespan in Different Trapping Structures Using an Integrated Microfluidic System. Advanced Materials Technologies 5, 2000655. https://doi.org/10.1002/admt.202000655

Ghavidel, A., Baxi, K., Ignatchenko, V., Prusinkiewicz, M., Arnason, T.G., Kislinger, T., Carvalho, C.E., Harkness, T.A.A., 2015. A Genome Scale Screen for Mutants with Delayed Exit from Mitosis: Ire1-Independent Induction of Autophagy Integrates ER Homeostasis into Mitotic Lifespan. PLOS Genetics 11, e1005429. https://doi.org/10.1371/journal.pgen.1005429

Gibson, D.G., Young, L., Chuang, R.-Y., Venter, J.C., Hutchison, C.A., Smith, H.O., 2009. Enzymatic assembly of DNA molecules up to several hundred kilobases. Nat Methods 6, 343–345. https://doi.org/10.1038/nmeth.1318

Gladyshev, V.N., 2021. The Ground Zero of Organismal Life and Aging. Trends in Molecular Medicine 27, 11–19. https://doi.org/10.1016/j.molmed.2020.08.012

Hansen, M., Rubinsztein, D.C., Walker, D.W., 2018. Autophagy as a promoter of longevity: insights from model organisms. Nat Rev Mol Cell Biol 19, 579–593. https://doi.org/10.1038/s41580-018-0033-y

Higuchi-Sanabria, R., Pernice, W.M.A., Vevea, J.D., Alessi Wolken, D.M., Boldogh, I.R., Pon, L.A., 2014. Role of asymmetric cell division in lifespan control in Saccharomyces cerevisiae. FEMS Yeast Res 14, 1133–1146. https://doi.org/10.1111/1567-1364.12216

Hughes, A.L., Gottschling, D.E., 2012. An early age increase in vacuolar pH limits mitochondrial function and lifespan in yeast. Nature 492, 261–265. https://doi.org/10.1038/nature11654

Ichimura, Y., Kirisako, T., Takao, T., Satomi, Y., Shimonishi, Y., Ishihara, N., Mizushima, N., Tanida, I., Kominami, E., Ohsumi, M., Noda, T., Ohsumi, Y., 2000. A ubiquitin-like system mediates protein lipidation. Nature 408, 488–492. https://doi.org/10.1038/35044114

Ide, S., Miyazaki, T., Maki, H., Kobayashi, T., 2010. Abundance of Ribosomal RNA Gene Copies Maintains Genome Integrity. Science 327, 693–696. https://doi.org/10.1126/science.1179044

Jin, M., Li, Y., O'Laughlin, R., Bittihn, P., Pillus, L., Tsimring, L.S., Hasty, J., Hao, N., 2019. Divergent Aging of Isogenic Yeast Cells Revealed through Single-Cell Phenotypic Dynamics. Cell Systems 8, 242-253.e3. https://doi.org/10.1016/j.cels.2019.02.002

Jo, M.C., Liu, W., Gu, L., Dang, W., Qin, L., 2015. High-throughput analysis of yeast replicative aging using a microfluidic system. Proceedings of the National Academy of Sciences 112, 9364–9369. https://doi.org/10.1073/pnas.1510328112

Jones, D.L., 2007. Aging and the Germ Line: Where Mortality and Immortality Meet. Stem Cell Rev 3, 192–200. https://doi.org/10.1007/s12015-007-0009-3

Kaeberlein, M., Kirkland, K.T., Fields, S., Kennedy, B.K., 2004. Sir2-Independent Life Span Extension by Calorie Restriction in Yeast. PLoS Biol 2, e296. https://doi.org/10.1371/journal.pbio.0020296

Kaeberlein, M., McVey, M., Guarente, L., 1999. The SIR2/3/4 complex and SIR2 alone promote longevity in Saccharomyces cerevisiae by two different mechanisms. Genes Dev 13, 2570–2580. https://doi.org/10.1101/gad.13.19.2570

Kamber, R.A., Shoemaker, C.J., Denic, V., 2015. Receptor-bound targets of selective autophagy use a scaffold protein to activate the Atg1 kinase. Mol Cell 59, 372–381. https://doi.org/10.1016/j.molcel.2015.06.009

Kane, S.M., Roth, R., 1974. Carbohydrate Metabolism During Ascospore Development in Yeast. Journal of Bacteriology 118, 8–14. https://doi.org/10.1128/jb.118.1.8-14.1974

Kanki, T., Wang, K., Cao, Y., Baba, M., Klionsky, D.J., 2009. Atg32 Is a Mitochondrial Protein that Confers Selectivity during Mitophagy. Developmental Cell 17, 98–109. https://doi.org/10.1016/j.devcel.2009.06.014

Kim, D.Y., Shin, J.Y., Lee, J.E., Kim, H.N., Chung, S.J., Yoo, H.S., Kim, S.J., Cho, H.J., Lee, E.-J., Nam, S.J., Kim, S.H., Jang, J., Lee, S.E., Lee, P.H., 2023. A selective ER-phagy exerts neuroprotective effects via modulation of α-synuclein clearance in parkinsonian models. Proceedings of the National Academy of Sciences 120, e2221929120. https://doi.org/10.1073/pnas.2221929120

King, G.A., Goodman, J.S., Schick, J.G., Chetlapalli, K., Jorgens, D.M., McDonald, K.L., Ünal, E., 2019. Meiotic cellular rejuvenation is coupled to nuclear remodeling in budding yeast. eLife 8, e47156. https://doi.org/10.7554/eLife.47156

Kobayashi, O., Suda, H., Ohtani, T., Sone, H., 1996. Molecular cloning and analysis of the dominant flocculation geneFLO8 fromSaccharomyces cerevisiae. Molec. Gen. Genet. 251, 707–715. https://doi.org/10.1007/BF02174120

Kobayashi, T., Ganley, A.R.D., 2005. Recombination Regulation by Transcription-Induced Cohesin Dissociation in rDNA Repeats. Science 309, 1581–1584. https://doi.org/10.1126/science.1116102

Kobayashi, T., Horiuchi, T., Tongaonkar, P., Vu, L., Nomura, M., 2004. *SIR2* Regulates Recombination between Different rDNA Repeats, but Not Recombination within Individual rRNA Genes in Yeast. Cell 117, 441–453. https://doi.org/10.1016/S0092-8674(04)00414-3

Koch, B.A., Staley, E., Jin, H., Yu, H.-G., 2020. The ESCRT-III complex is required for nuclear pore complex sequestration and regulates gamete replicative lifespan in budding yeast meiosis. Nucleus 11, 219–236. https://doi.org/10.1080/19491034.2020.1812872

Kondo-Okamoto, N., Noda, N.N., Suzuki, S.W., Nakatogawa, H., Takahashi, I., Matsunami, M., Hashimoto, A., Inagaki, F., Ohsumi, Y., Okamoto, K., 2012. Autophagy-related Protein 32 Acts as Autophagic Degron and Directly Initiates Mitophagy*. Journal of Biological Chemistry 287, 10631–10638. https://doi.org/10.1074/jbc.M111.299917

Lee, M.B., Dowsett, I.T., Carr, D.T., Wasko, B.M., Stanton, S.G., Chung, M.S., Ghodsian, N., Bode, A., Kiflezghi, M.G., Uppal, P.A., Grayden, K.A., Elala, Y.C., Tang, T.T., Tran, N.H.B., Tran, T.H.B., Diep, A.B., Hope, M., Promislow, D.E.L., Kennedy, S.R., Kaeberlein, M., Herr, A.J., 2019. Defining the impact of mutation accumulation on replicative lifespan in yeast using cancer-associated mutator phenotypes. Proc Natl Acad Sci U S A 116, 3062–3071. https://doi.org/10.1073/pnas.1815966116

Li, Y., Jiang, Y., Paxman, J., O'Laughlin, R., Klepin, S., Zhu, Y., Pillus, L., Tsimring, L.S., Hasty, J., Hao, N., 2020. A programmable fate decision landscape underlies single-cell aging in yeast. Science 369, 325–329. https://doi.org/10.1126/science.aax9552

Liu, P., Young, T.Z., Acar, M., 2015. Yeast Replicator: A High-Throughput Multiplexed Microfluidics Platform for Automated Measurements of Single-Cell Aging. Cell Reports 13, 634–644. https://doi.org/10.1016/j.celrep.2015.09.012

Longtine, M.S., Mckenzie III, A., Demarini, D.J., Shah, N.G., Wach, A., Brachat, A., Philippsen, P., Pringle, J.R., 1998. Additional modules for versatile and economical PCR-based gene deletion and modification in Saccharomyces cerevisiae. Yeast 14, 953–961. https://doi.org/10.1002/(SICI)1097-0061(199807)14:10%253C953::AID-YEA293%253E3.0.CO;2-U

Maklakov, A.A., Immler, S., 2016. The Expensive Germline and the Evolution of Ageing. Current Biology 26, R577–R586. https://doi.org/10.1016/j.cub.2016.04.012

Matos, J., Lipp, J.J., Bogdanova, A., Guillot, S., Okaz, E., Junqueira, M., Shevchenko, A., Zachariae, W., 2008. Dbf4-Dependent Cdc7 Kinase Links DNA Replication to the Segregation of Homologous Chromosomes in Meiosis I. Cell 135, 662–678. https://doi.org/10.1016/j.cell.2008.10.026

Matsuura, A., Tsukada, M., Wada, Y., Ohsumi, Y., 1997. Apg1p, a novel protein kinase required for the autophagic process in *Saccharomyces cerevisiae*. Gene 192, 245–250. https://doi.org/10.1016/S0378-1119(97)00084-X

Mizushima, N., Levine, B., Cuervo, A.M., Klionsky, D.J., 2008. Autophagy fights disease through cellular self-digestion. Nature 451, 1069–1075. https://doi.org/10.1038/nature06639

Mochida, K., Oikawa, Y., Kimura, Y., Kirisako, H., Hirano, H., Ohsumi, Y., Nakatogawa, H., 2015. Receptor-mediated selective autophagy degrades the endoplasmic reticulum and the nucleus. Nature 522, 359–362. https://doi.org/10.1038/nature14506

Mortimer, R.K., Johnston, J.R., 1959. Life Span of Individual Yeast Cells. Nature 183, 1751–1752. https://doi.org/10.1038/1831751a0

Murphy, S.M., Davidson, G.L., Brandner, S., Houlden, H., Reilly, M.M., 2012. Mutation in FAM134B causing severe hereditary sensory neuropathy. J Neurol Neurosurg Psychiatry 83, 119–120. https://doi.org/10.1136/jnnp.2010.228965

Neiman, A.M., 2011. Sporulation in the Budding Yeast Saccharomyces cerevisiae. Genetics 189, 737–765. https://doi.org/10.1534/genetics.111.127126

Neiman, A.M., 2005. Ascospore Formation in the Yeast Saccharomyces cerevisiae. Microbiol Mol Biol Rev 69, 565–584. https://doi.org/10.1128/MMBR.69.4.565-584.2005

Nyström, T., Liu, B., 2014. Protein quality control in time and space – links to cellular aging. FEMS Yeast Res 14, 40–48. https://doi.org/10.1111/1567-1364.12095

Okamoto, K., Kondo-Okamoto, N., Ohsumi, Y., 2009. Mitochondria-Anchored Receptor Atg32 Mediates Degradation of Mitochondria via Selective Autophagy. Developmental Cell 17, 87–97. https://doi.org/10.1016/j.devcel.2009.06.013

Otto, G.M., Brar, G.A., 2022. Developmentally regulated selective autophagy determines ER inheritance by gametes. Autophagy 18, 1732–1733. https://doi.org/10.1080/15548627.2022.2040315

Otto, G.M., Cheunkarndee, T., Leslie, J.M., Brar, G.A., 2021. Programmed cortical ER collapse drives selective ER degradation and inheritance in yeast meiosis. Journal of Cell Biology 220, e202108105. https://doi.org/10.1083/jcb.202108105

Padmore, R., Cao, L., Kleckner, N., 1991. Temporal comparison of recombination and synaptonemal complex formation during meiosis in S. cerevisiae. Cell 66, 1239–1256. https://doi.org/10.1016/0092-8674(91)90046-2

Powers, E.N., Chan, C., Doron-Mandel, E., Llacsahuanga Allcca, L., Kim Kim, J., Jovanovic, M., Brar, G.A., 2022. Bidirectional promoter activity from expression cassettes can drive off-target repression of neighboring gene translation. eLife 11, e81086. https://doi.org/10.7554/eLife.81086

Rubinsztein, D.C., Mariño, G., Kroemer, G., 2011. Autophagy and Aging. Cell 146, 682–695. https://doi.org/10.1016/j.cell.2011.07.030

Saliba, E., Evangelinos, M., Gournas, C., Corrillon, F., Georis, I., André, B., 2018. The yeast H+-ATPase Pma1 promotes Rag/Gtr-dependent TORC1 activation in response to H+-coupled nutrient uptake. eLife 7, e31981. https://doi.org/10.7554/eLife.31981

Sato, K., Sato, M., Nakano, A., 1997. Rer1p as common machinery for the endoplasmic reticulum localization of membrane proteins. Proceedings of the National Academy of Sciences 94, 9693–9698. https://doi.org/10.1073/pnas.94.18.9693

Sawyer, E.M., Joshi, P.R., Jorgensen, V., Yunus, J., Berchowitz, L.E., Ünal, E., 2018. Developmental regulation of an organelle tether coordinates mitochondrial remodeling in meiosis. J Cell Biol 218, 559–579. https://doi.org/10.1083/jcb.201807097

Schindelin, J., Arganda-Carreras, I., Frise, E., Kaynig, V., Longair, M., Pietzsch, T., Preibisch, S., Rueden, C., Saalfeld, S., Schmid, B., Tinevez, J.-Y., White, D.J., Hartenstein, V., Eliceiri, K., Tomancak, P., Cardona, A., 2012. Fiji: an open-source platform for biological-image analysis. Nature Methods 9, 676–682. https://doi.org/10.1038/nmeth.2019

Schlesser, A., Ulaszewski, S., Ghislain, M., Goffeau, A., 1988. A second transport ATPase gene in Saccharomyces cerevisiae. Journal of Biological Chemistry 263, 19480–19487. https://doi.org/10.1016/S0021-9258(19)77659-5

Serrano, R., Kielland-Brandt, M.C., Fink, G.R., 1986. Yeast plasma membrane ATPase is essential for growth and has homology with (Na+ + K+), K+- and Ca2+-ATPases. Nature 319, 689–693. https://doi.org/10.1038/319689a0

Simonsen, A., Cumming, R.C., Brech, A., Isakson, P., Schubert, D.R., Finley, K.D., 2008. Promoting basal levels of autophagy in the nervous system enhances longevity and oxidant resistance in adult Drosophila. Autophagy 4, 176–184. https://doi.org/10.4161/auto.5269

Sinclair, D.A., Guarente, L., 1997. Extrachromosomal rDNA Circles— A Cause of Aging in Yeast. Cell 91, 1033–1042. https://doi.org/10.1016/S0092-8674(00)80493-6

Sing, Tina L., Brar, G.A., Ünal, E., 2022. Gametogenesis: Exploring an Endogenous Rejuvenation Program to Understand Cellular Aging and Quality Control. Annu. Rev. Genet. 56, 89–112. https://doi.org/10.1146/annurev-genet-080320-025104

Sing, Tina L, Conlon, K., Lu, S.H., Madrazo, N., Morse, K., Barker, J.C., Hollerer, I., Brar, G.A., Sudmant, P.H., Ünal, E., 2022. Meiotic cDNA libraries reveal gene truncations and mitochondrial proteins important for competitive fitness in Saccharomyces cerevisiae. Genetics 221, iyac066. https://doi.org/10.1093/genetics/iyac066

Smeal, T., Claus, J., Kennedy, B., Cole, F., Guarente, L., 1996. Loss of Transcriptional Silencing Causes Sterility in Old Mother Cells of S. cerevisiae. Cell 84, 633–642. https://doi.org/10.1016/S0092-8674(00)81038-7

Smelick, C., Ahmed, S., 2005. Achieving immortality in the *C. elegans* germline. Ageing Research Reviews 4, 67–82. https://doi.org/10.1016/j.arr.2004.09.002

Suda, Y., Nakanishi, H., Mathieson, E.M., Neiman, A.M., 2007. Alternative Modes of Organellar Segregation during Sporulation in Saccharomyces cerevisiae. Eukaryotic Cell 6, 2009–2017. https://doi.org/10.1128/ec.00238-07

Thayer, N.H., Robles, M., Xu, J., Schinski, E.L., Hotz, M., Keyser, R., Millett-Sikking, A., Okreglak, V., Rogers, J.V., Waite, A.J., Wranik, B.J., York, A.G., McIsaac, R.S., Gottschling, D.E., 2022. The Yeast Lifespan Machine: a microfluidic platform for automated replicative lifespan measurements. https://doi.org/10.1101/2022.02.14.480146

Tsukada, M., Ohsumi, Y., 1993. Isolation and characterization of autophagy-defective mutants of Saccharomyces cerevisiae. FEBS Letters 333, 169–174. https://doi.org/10.1016/0014-5793(93)80398-E

Tyler, J.K., Johnson, J.E., 2018. The role of autophagy in the regulation of yeast life span. Ann N Y Acad Sci 1418, 31–43. https://doi.org/10.1111/nyas.13549

Ünal, E., Amon, A., 2011. Gamete formation resets the aging clock in yeast. Cold Spring Harb Symp Quant Biol 76, 73–80. https://doi.org/10.1101/sqb.2011.76.011379

Ünal, E., Kinde, B., Amon, A., 2011. Gametogenesis Eliminates Age-Induced Cellular Damage and Resets Life Span in Yeast. Science 332, 1554–1557. https://doi.org/10.1126/science.1204349

Wen, F.-P., Guo, Y.-S., Hu, Y., Liu, W.-X., Wang, Q., Wang, Y.-T., Yu, H.-Y., Tang, C.-M., Yang, J., Zhou, T., Xie, Z.-P., Sha, J.-H., Guo, X., Li, W., 2016. Distinct temporal requirements for autophagy and the proteasome in yeast meiosis. Autophagy 12, 671–688. https://doi.org/10.1080/15548627.2016.1149659

Xu, L., Ajimura, M., Padmore, R., Klein, C., Kleckner, N., 1995. NDT80, a meiosis-specific gene required for exit from pachytene in Saccharomyces cerevisiae. Mol Cell Biol 15, 6572–6581. https://doi.org/10.1128/mcb.15.12.6572

Yamashita, Y.M., 2023. Asymmetric Stem Cell Division and Germline Immortality. Annual Review of Genetics 57, 181–199. https://doi.org/10.1146/annurev-genet-022123-040039

Supplementary information

Table S1. Strain Table

Strain number yÜB[1]	MAT	Genotype[2,3]	Source[4]
SK1	Strain background	*ho::LYS2, lys2, leu2::hisG, ura3, his3::hisG, trp1::hisG*	
13	*MATa*	WT	
14	*MATα*	WT	
15	*MATa/α* (diploid)	WT	
29559	diploid	*trp1::pPma2-Pma2-eGFP::TRP1, HTB1-mCherry-HISMX6* (heterozygote with *his3::hisG*)	this study
42275	diploid	*trp1::pPma2-Pma2-eGFP::TRP1, ste5::NatR-pTet07.1-STE5, ura3::pRNR2-TetR-Tup1, pTetO7.1-TetR::URA3, flo8Δ, Amn1^{D368V}*	this study
42274	diploid	*trp1::pPma2-Pma2-eGFP::TRP1, ste5::NatR-pTet07.1-STE5, ura3::pRNR2-TetR-Tup1, pTetO7.1-TetR::URA3, flo8Δ, Amn1^{D368}*	this study
43791	diploid	*sir2Δ::KanMX* (heterozygote with *sir2Δ::HISMX6) trp1::pPma2-Pma2-eGFP::TRP1, ste5::NatR-pTet07.1-STE5, ura3::pRNR2-TetR-Tup1, pTetO7.1-TetR::URA3, flo8Δ, Amn1^{D368}*	this study
43766	diploid	*fob1Δ::KanMX, trp1::pPma2-Pma2-eGFP::TRP1, ste5::NatR-pTet07.1-STE5, ura3::pRNR2-TetR-Tup1, pTetO7.1-TetR::URA3, flo8Δ, Amn1^{D368}*	this study
45418	diploid	*sir2Δ::KanMX, sir2Δ::HISMX6, leu2::pRIM4-SIR2-V5::LEU2* (heterozygote with *leu2::hisG*), *trp1::pPma2-Pma2-eGFP::TRP1, ste5::NatR-pTet07.1-STE5, ura3::pRNR2-TetR-Tup1, pTetO7.1-TetR::URA3, flo8Δ, Amn1^{D368}*	this study
48561	diploid	*atg11Δ::KanMX, trp1::pPma2-Pma2-eGFP::TRP1, ste5::NatR-pTet07.1-STE5, ura3::pRNR2-TetR-Tup1, pTetO7.1-TetR::URA3, flo8Δ, Amn1^{D368}*	this study
45501	diploid	*atg32Δ::KanMX, trp1::pPma2-Pma2-eGFP::TRP1, ste5::NatR-pTet07.1-STE5, ura3::pRNR2-TetR-Tup1, pTetO7.1-TetR::URA3, flo8Δ, Amn1^{D368}*	this study
48175	diploid	*atg33Δ::KanMX, trp1::pPma2-Pma2-eGFP::TRP1, ste5::NatR-pTet07.1-STE5, ura3::pRNR2-TetR-Tup1, pTetO7.1-TetR::URA3, flo8Δ, Amn1^{D368}*	this study
48216	diploid	*atg32Δ::KanMX, atg33Δ::KanMX, trp1::pPma2-Pma2-eGFP::TRP1, ste5::NatR-pTet07.1-STE5, ura3::pRNR2-TetR-Tup1, pTetO7.1-TetR::URA3, flo8Δ, Amn1^{D368}*	this study
44411	diploid	*atg39Δ::KanMX, trp1::pPma2-Pma2-eGFP::TRP1, ste5::NatR-pTet07.1-STE5, ura3::pRNR2-TetR-Tup1, pTetO7.1-TetR::URA3, flo8Δ, Amn1^{D368}*	this study

42753	diploid	*atg40Δ::KanMX, trp1::pPma2-Pma2-eGFP::TRP1, ste5::NatR-pTet07.1-STE5, ura3::pRNR2-TetR-Tup1, pTetO7.1-TetR::URA3, flo8Δ, Amn1^{D368}*	this study
45176	diploid	*atg39Δ::KanMX, atg40Δ::KanMX, trp1::pPma2-Pma2-eGFP::TRP1, ste5::NatR-pTet07.1-STE5, ura3::pRNR2-TetR-Tup1, pTetO7.1-TetR::URA3, flo8Δ, Amn1^{D368}*	this study
47417	diploid	*leu2::LEU2, atg39Δ::KanMX, atg40Δ::KanMX, trp1::pPma2-Pma2-eGFP::TRP1, ste5::NatR-pTet07.1-STE5, ura3::pRNR2-TetR-Tup1, pTetO7.1-TetR::URA3, flo8Δ, Amn1^{D368}*	this study
48312	diploid	*leu2::pNDT80-ATG40-V5::LEU2, atg39Δ::KanMX, atg40Δ::KanMX, trp1::pPma2-Pma2-eGFP::TRP1, ste5::NatR-pTet07.1-STE5, ura3::pRNR2-TetR-Tup1, pTetO7.1-TetR::URA3, flo8Δ, Amn1^{D368}*	this study
14554	diploid	*atg40::ATG40-3V5-KanMX*	(Otto et al., 2021)

[1]Strains are listed according to Figure order.
[2]Alleles are separated by commas.
[3]All indicated alleles in diploids are homozygous, unless otherwise specified.
[4]Previously generated alleles are further described elsewhere (see Methods).

Table S2 Plasmids

Plasmid number (pÜB)	Construct[1]	Backbone	Bacterial selection	Source / Reference
1	*KanMX6*	pFA6a	Ampicilin	(Longtine et al., 1998)
153	*NatMX4*	pFA6a	Ampicilin	(Longtine et al., 1998)
2693	*NatMX4_ PtetO7.1*	pFA6a	Ampicilin	Adapted from (Azizoglu et al., 2021)
2255	*kanMX6-ins1*	pFA6a	Ampicilin	(Powers et al., 2022)
2309	*his3MX6-ins3*	pFA6a	Ampicilin	(Powers et al., 2022)
1905	*PPMA2-PMA2-eGPF_LEU2*	pNH604	Ampicilin	This study
2991	*PRIM4-SIR2-V5_LEU2*	pLC605	Ampicilin	This study
3076	*PNDT80-ATG40-V5_LEU2*	pÜB2991	Ampicilin	This study
2371	*PRNR2-TetR-TUP1_PtetO7.1-TetR_URA3*	pSV606	Ampicilin	Adapted from (Azizoglu et al., 2021)

[1]Underscores indicate separation between plasmid elements (e.g. construct and selection cassette)

Table S3. Primers

Allele	Forward primer	Reverse primer	Template
pTETO-STE5	CTAAAAAAGGAAGATACA GGATACAGCGGAAACAAC TTTTAAcgtacgctgcaggtcgac	TGTGAAAAGGGGAAACTAT ATTGTCTGTAGGAGTTTCCA Tcatcgatgaattctctgtcg	pÜB2693
sir2Δ	CATTCAAACCATTTTTCCC TCATCGGCACATTAAAGCT GGcggatccccgggttaattaa	TATTAATTTGGCACTTTTAA ATTATTAAATTGCCTTCTACg aattcgagctcgtttaaac	pÜB2255 & pÜB2309
fob1Δ	TTAACGATTGTGTGAGTGT GAATTTGTGCTGAGGATA ACAcggatccccgggttaattaa	TGGAGATCAAACAAGAGAC TTTGGCACATCAATGGAATT Gcggatccccgggttaattaa	pÜB1
atg11Δ	GTTGTTCGGAAAGTACTTC TTTTATTTTCTTTTATGCAT Ccggatccccgggttaattaa	AATTAAAATCTTGTCATTTG TGACAAACGTTTAGCACTGT gaattcgagctcgtttaaac	pÜB2255
atg33Δ	TACTACTTCACGATATACA GAAGTAAAAACATATAAA AAGcggatccccgggttaattaa	CTACAAATTCTTGTAGAGAT AAATACGTGAACGAGAAAC Agaattcgagctcgtttaaac	pÜB2255

[1] Lowercase letters indicate common primer adaptor sequences(Longtine et al., 1998; Powers et al., 2022), uppercase letters indicate primer tail introducing homology to target gene locus.
[2] pÜB plasmids can be found in Table S2.